SANDIA REPORT

SAND88—3050 • UC—814
Unlimited Release
Printed May 1991

Yucca Mountain Site Characterization Project

Calculation of Heat Capacities for Tuffaceous Units from the Unsaturated Zone at Yucca Mountain, Nevada

Francis B. Nimick, James R. Connolly

Prepared by
Sandia National Laboratories
Albuquerque, New Mexico 87185 and Livermore, California 94550
for the United States Department of Energy
under Contract DE-AC04-76DP00789

"Prepared by Yucca Mountain Site Characterization Project (YMSCP) participants as part of the Civilian Radioactive Waste Management Program (CRWM). The YMSCP is managed by the Yucca Mountain Project Office of the U.S. Department of Energy, Nevada Operations Office (DOE/NV). YMSCP work is sponsored by the Office of Geologic Repositories (OGR) of the DOE Office of Civilian Radioactive Waste Management (OCRWM)."

Issued by Sandia National Laboratories, operated for the United States Department of Energy by Sandia Corporation.

Available to DOE and DOE contractors from
Office of Scientific and Technical Information
PO Box 62
Oak Ridge, TN 37831

Prices available from (615) 576-8401, FTS 626-8401

Available to the public from
National Technical Information Service
US Department of Commerce
5285 Port Royal Rd
Springfield, VA 22161

NTIS price codes
Printed copy: A05
Microfiche copy: A01

DISCLAIMER

Portions of this document may be illegible in electronic image products. Images are produced from the best available original document.

SAND--88-3050

DE91 012366

SAND88-3050
Unlimited Release
Printed May 1991

Calculation of Heat Capacities for Tuffaceous Units from the Unsaturated Zone at Yucca Mountain, Nevada

Francis B. Nimick

Geotechnical Projects Division
Sandia National Laboratories
P.O. Box 5800
Albuquerque, NM 87185

James R. Connolly

Department of Geology
Institute of Meteoritics
University of New Mexico
Albuquerque, NM 87131

ABSTRACT

In the absence of experimentally determined heat capacity data, bulk-chemical analyses of 20 samples of tuffs from Yucca Mountain have been used to calculate heat capacities of the solid components of the tuffs as a function of temperature. These calculated values, which should be validated by experiments as soon as practicable, have been combined with data on grain density, matrix porosity, lithophysal-cavity abundance, mineral abundance, in situ saturation, and the properties of water to estimate rock-mass thermal capacitances. In general, thermal capacitance is higher for tuffs with higher porosity for the same pore fluid; saturated tuffs have higher thermal capacitances than partially saturated or dry tuffs. The heat capacity of the solid components provides a secondary contribution.

The task for which this report was prepared was a QA Level I Task under WBS 1.2.4.2.1.3.S. However, the QA level was proposed to be changed to III, and the report was prepared as a Level III activity because of interim approval of the change in level. Thus, although QA Level I is the only officially approved level, this is not considered to be a Level I report. The data used were all either NQ or QA III. This work relates to SCP Activity 8.3.1.15.1.1.2, "Volumetric Heat Capacity Characterization."

CONTENTS

CONTENTS
(Concluded)

TABLES

FIGURES

1.0 INTRODUCTION

Yucca Mountain, located in and near the southwest corner of the Nevada Test Site (NTS) in southern Nye County, Nevada (Figure 1), has been identified by the Department of Energy (DOE) as a potential site for the disposal of radioactive waste. Responsibility for studying the suitability of Yucca Mountain as a disposal site rests with the Yucca Mountain Site Characterization Project (YMP), administered by the DOE offices in Las Vegas, Nevada. Sandia National Laboratories (SNL) is one of the primary YMP participants and has responsibilities for performance assessment, repository design, and determination of the thermal and mechanical properties of some of the tuff units from Yucca Mountain.

Figure 2 is a summary of the younger stratigraphic units present at Yucca Mountain. All of the units shown in Figure 2 are tuffaceous, but the lithologies vary from bedded and massive ash-fall and pyroclastic surge deposits, reworked tuffs and volcaniclastic sands, through nonwelded vitric or zeolitized ash-flow tuffs to densely welded devitrified or vitric ash flows. The Topopah Spring Member of the Paintbrush Tuff is the target horizon for waste emplacement.

One set of rock properties to be measured includes those involved in heat transfer. Heat capacity is one of the heat transfer properties for which data are required. To date, no heat capacity experiments have been performed, primarily because of the belief that heat capacity could be estimated to the necessary accuracy using existing published data (Tillerson and Nimick, 1984). In earlier work, a constant value was assumed for the heat capacity of the solid portion of the tuffaceous rocks. This value then was combined with data on porosity, saturation, and the heat capacity of water to calculate rock-mass heat capacities.

The same general approach is still useful with one exception. Rather than assuming a constant value for the heat capacity of solids, chemical and mineralogic data are combined with published heat capacity data (including temperature dependence) to estimate sample-specific values for the heat capacities of the solid portions of tuffaceous rocks. This is

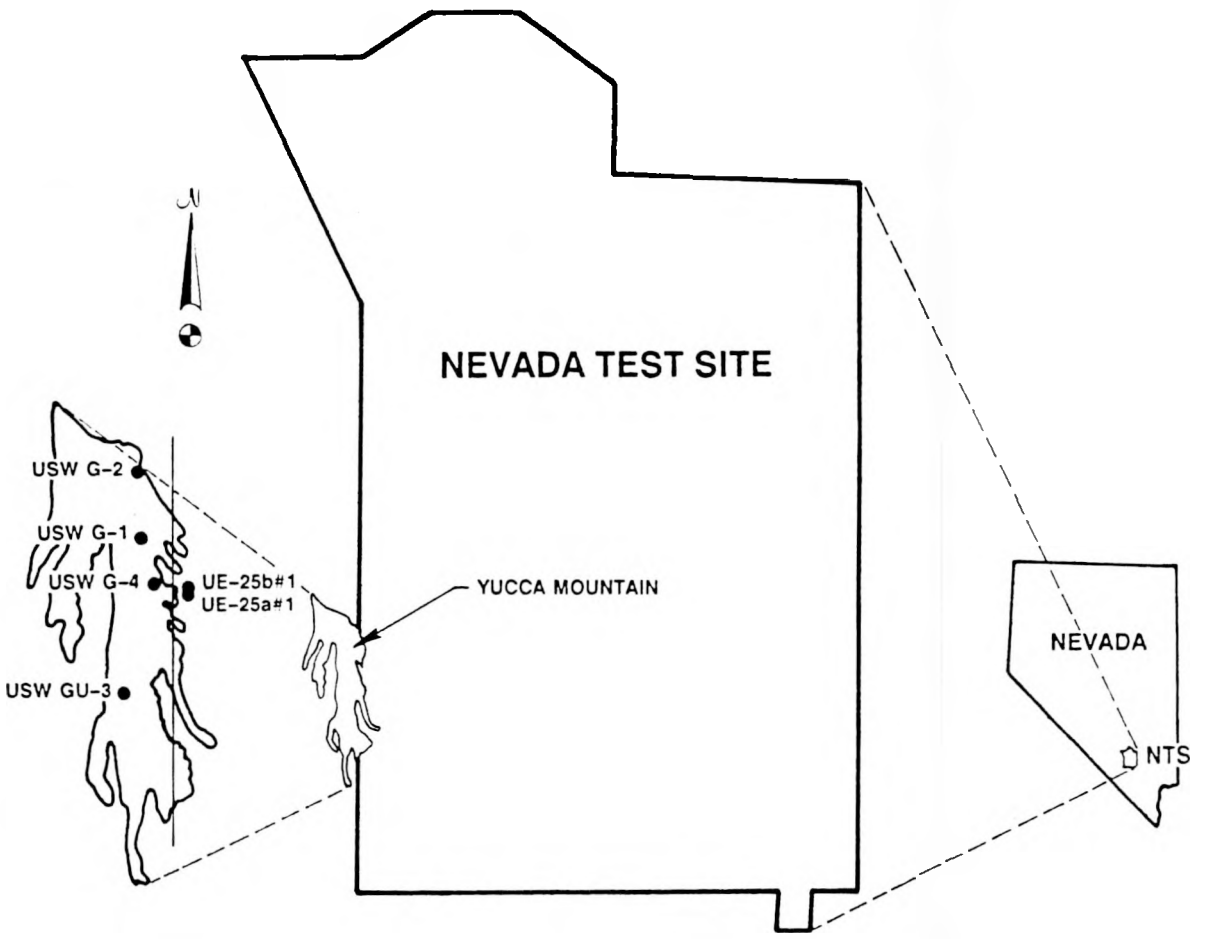

Figure 1. Locations of the Nevada Test Site, Yucca Mountain, and Existing Deep Coreholes

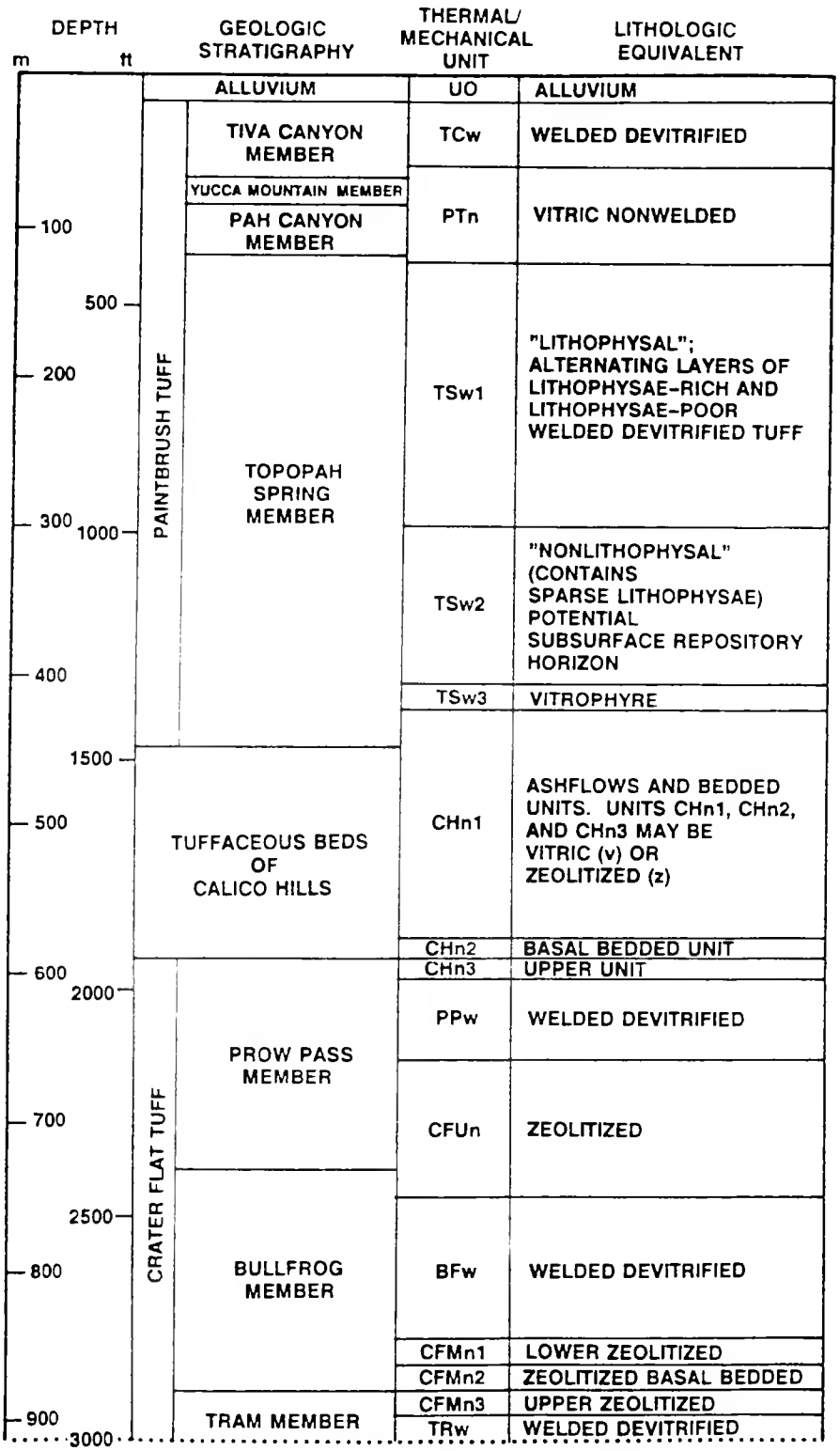

Figure 2. Stratigraphy of Tuffaceous Units at Yucca Mountain (Thicknesses of units are averages for the coreholes shown in Figure 1.)

now possible for the tuffaceous units from Yucca Mountain because Connolly and Nimick (1990) have provided a summary of data on 20 samples of these units from which heat capacities can be estimated.

Section 2.0 of this report provides a detailed description of the process of heat capacity estimation for the 20 samples. An analysis of the values estimated in Section 2.0 is presented in Section 3.0; the culmination of the analysis is a set of recommended rock-mass heat capacities for the thermal/mechanical units in the unsaturated zone at Yucca Mountain. Section 4.0 is a brief discussion of the assumptions made during the analysis.

2.0 ESTIMATION OF HEAT CAPACITIES OF SOLIDS

2.1 General Approach to the Problem

Heat capacity is a fundamental thermodynamic property of materials. Heat capacity at constant-pressure (the main contributor to the models proposed in this report) is strictly defined as the partial derivative of enthalpy with temperature, holding pressure constant. However, as used in this report and predicted by the modeling techniques and assumptions discussed in the later sections, heat capacity is not the strictly defined thermodynamic variety. Instead, "effective" heat capacities are derived which include all contributions from thermodynamics, reaction kinetics and heat absorbed or released during phase transitions. Thus, heat capacity as defined for this report is the quantity of heat required to change the temperature of a unit of material by one degree. Heat capacity may be defined on either a mass, volume, or molar basis. Many of the data in the literature are reported in J/(mol•K) or cal/(mol•K). For this study, such data are converted to J/(g•K) by dividing by the appropriate formula weight (g/mol) and using the conversion 1 J = 0.239 cal when necessary.

Several experiment techniques are commonly used to determine the heat capacities of minerals or of oxide components of minerals. These include low-temperature (generally <500°C) calorimetry and, at higher temperatures, measurement of heats of solution. Heat capacity at constant pressure (C_p) is calculated from experiment data and is represented as a function of absolute temperature by an equation involving various terms in different powers of temperature. The equation used here, which includes all terms commonly found in the literature, is

$$C_p = A + BT + CT^{1/2} + DT^2 + ET^{-1/2} + FT^{-1} + GT^{-2} \quad , \qquad (1)$$

where T is absolute temperature and A, B, C, etc., are empirically derived constants.

No experiment data are available for the heat capacities of the tuffaceous rocks from Yucca Mountain. However, values can be estimated in

several ways from existing data. Equations of the form of Equation 1 (or a reduced version thereof) exist for all of the common rock-forming oxides (SiO_2, CaO, Al_2O_3, etc.) and for many minerals that are common in silicate rocks. The heat capacities of either the oxides or of the minerals may be summed according to

$$C_p = \sum_i x_i \, C_{p,i} \quad , \tag{2}$$

where x_i is the fraction of the i^{th} oxide (or mineral phase) in the rock, and $C_{p,i}$ is the corresponding heat capacity. Such summations are based on Kopp's rule (Kopp, 1864) which holds that the heat capacity of a solid compound is equal to the sum of the heat capacities of its constituent elements.* Kopp's rule is generally accepted as providing a simple approximation of the heat capacities of most substances (Nash, 1971; Robinson and Haas, 1983). In the discussion that follows, use of Equation 2 with heat capacity data for oxides is called the oxide-summation method, and Equation 2 used with mineral heat capacity data is called the mineral-summation method.

A third summation method--the fictive-oxide mineral-component method--is proposed by Robinson and Haas (1983) as a significantly more accurate estimator of the heat capacities of solids. This method was considered, but has not been used in this study for several reasons. First, very detailed information regarding the composition and structure of constituent minerals is required, and this information generally is not available without very detailed x-ray mineralogical studies. Second, very accurate estimates of weight fractions of the minerals are required to make the results significantly better than those for the other methods. The

---

*This is an approximation because, if it were strictly true, $\Delta C_p = 0$ for any chemical reaction, which is not the case. Other contributions to heat capacity arise from order/disorder phenomena in crystals, rotational movement of atoms, and magnetic and electric effects. However, at temperatures significantly removed from absolute zero, the approximation usually is quite good.

information on weight fractions is not easily obtainable for the samples used in this study, so that the errors in the estimation of weight fractions of the minerals are probably larger than the errors in values of C_p calculated by the other methods.

2.2 Data Used in Heat-Capacity Estimation

Most of the heat capacity data used for this study are taken from published thermodynamic tables, chiefly Robie et al. (1978). The oxides used in the oxide-summation method are SiO_2, TiO_2, Al_2O_3, Fe_2O_3, FeO, MnO, MgO, CaO, Na_2O, K_2O, P_2O_5, and H_2O. Mineral phases considered for use in the mineral-summation method are quartz, corundum, orthoclase, albite, anorthite, hypersthene, magnetite, hematite, ilmenite, rutile, apatite, clinoptilolite, montmorillonite (clay), and H_2O. Relevant bulk-chemical, mineralogic, and petrologic data for 20 samples of tuffaceous rocks are presented in Connolly and Nimick (1990).

The heat capacity equations calculated here are based on inputs using normalized chemical analyses. For the purposes of these initial estimates, the standard assumption was made that H_2O^- represented water present in pores and adsorbed on particle surfaces, and that H_2O^+ includes all structural water in the constituent minerals. This assumption needs to be tested by thermogravimetric analysis (TGA) of the samples, which will measure the amount of water lost from the samples at particular temperatures, because it is possible that some water contained in zeolite channels may be erroneously measured as H_2O^-. The normalized analyses omit H_2O^- and normalize the remaining oxide components, including H_2O^+, to 100%. The whole-rock chemical analyses (from Connolly and Nimick, 1990) and normalized analyses for all samples are given in Table 1.

2.3 Mineral-Summation Method

As stated in Section 2.1, the fictive-oxide mineral-component method of heat capacity estimation was not used for this study because required information was not available. A similar conclusion has been reached concerning the mineral-summation method, even though the potential

TABLE 1

CHEMICAL ANALYSES OF SAMPLES USED IN ESTIMATION OF HEAT CAPACITY

Constituent	A1-1518.9	G1-504.6	G1-1151.1	G1-1288.9	G1-1796.4	G2-1646.8
			Original Analyses* (wt%)			
SiO_2	69.30	74.16	75.64	74.17	64.87	73.44
TiO_2	0.08	0.18	0.12	0.11	0.33	0.11
Al_2O_3	11.88	13.64	13.06	12.76	13.96	12.70
Fe_2O_3	0.85	1.12	0.70	0.60	2.86	0.63
FeO	<0.01	<0.01	<0.01	0.34	<0.01	0.24
MnO	0.06	0.09	0.08	0.08	0.25	0.08
MgO	0.04	0.24	0.19	0.06	0.90	0.05
CaO	2.12	0.62	0.54	0.60	1.81	0.59
Na_2O	1.27	3.38	3.14	4.11	2.75	3.28
K_2O	4.22	5.10	4.80	3.66	3.59	4.60
P_2O_5	0.01	0.02	0.01	0.01	0.05	0.01
H_2O^+	6.46	0.82	0.89	3.28	5.13	3.93
H_2O^-	4.11	0.32	0.58	0.18	3.96	0.19
Total	100.39	99.68	99.75	99.96	100.47	99.84
			Normalized Analyses (wt%)			
SiO_2	71.97	74.64	76.27	74.33	67.22	73.70
TiO_2	0.08	0.18	0.12	0.11	0.34	0.11
Al_2O_3	12.34	13.73	13.17	12.79	14.46	12.74
Fe_2O_3	0.88	1.13	0.71	0.60	2.96	0.63
FeO	<0.01	<0.01	<0.01	0.34	<0.01	0.24
MnO	0.06	0.09	0.08	0.08	0.26	0.08
MgO	0.04	0.24	0.19	0.06	0.93	0.05
CaO	2.20	0.62	0.54	0.60	1.88	0.59
Na_2O	1.32	3.40	3.17	4.12	2.85	3.29
K_2O	4.38	5.13	4.84	3.67	3.72	4.62
P_2O_5	0.01	0.02	0.01	0.01	0.05	0.01
H_2O^+	6.71	0.83	0.90	3.29	5.32	3.94
Total	99.99	100.01	100.00	100.00	99.99	100.00

TABLE 1

CHEMICAL ANALYSES OF SAMPLES USED IN ESTIMATION OF HEAT CAPACITY (Continued)

Constituent	G2-1659.2	G2-1748.0	GU3-542.7	GU3-857.1	G4-329.4	G4-493.2	G4-965.2
			Original Analyses* (wt%)				
SiO_2	72.33	72.02	74.57	75.36	68.29	75.47	75.62
TiO_2	0.11	0.08	0.15	0.11	0.43	0.12	0.11
Al_2O_3	12.76	10.72	13.38	12.94	16.10	12.98	12.84
Fe_2O_3	0.69	0.65	1.19	1.06	2.04	1.07	0.99
FeO	0.16	0.03	<0.01	0.08	<0.01	<0.01	<0.01
MnO	0.08	0.07	0.09	0.08	0.10	0.08	0.08
MgO	0.06	0.07	0.10	0.11	0.28	0.17	0.13
CaO	0.88	1.60	0.53	0.53	1.06	0.55	0.54
Na_2O	2.77	1.75	3.63	3.54	4.40	3.40	3.30
K_2O	4.77	3.84	5.07	4.70	5.84	4.84	4.74
P_2O_5	0.01	0.01	0.01	0.01	0.07	0.01	0.01
H_2O^+	4.58	6.05	0.52	0.55	0.46	0.65	0.64
H_2O^-	0.70	3.00	0.12	0.14	0.00	0.46	0.48
Total	99.89	99.89	99.37	99.20	99.06	99.80	99.47
			Normalized Analyses (wt%)				
SiO_2	72.92	74.33	75.13	76.07	68.94	75.97	76.38
TiO_2	0.11	0.08	0.15	0.11	0.43	0.12	0.11
Al_2O_3	12.86	11.06	13.48	13.06	16.25	13.07	12.97
Fe_2O_3	0.70	0.67	1.20	1.07	2.06	1.08	1.00
FeO	0.16	0.03	<0.01	0.08	<0.01	<0.01	<0.01
MnO	0.08	0.07	0.09	0.08	0.10	0.08	0.08
MgO	0.06	0.07	0.11	0.11	0.28	0.17	0.13
CaO	0.89	1.65	0.53	0.54	1.07	0.55	0.55
Na_2O	2.79	1.81	3.66	3.57	4.44	3.42	3.33
K_2O	4.81	3.96	5.11	4.74	5.90	4.87	4.79
P_2O_5	0.01	0.01	0.02	0.01	0.07	0.01	0.01
H_2O^+	4.62	6.24	0.52	0.56	0.46	0.65	0.65
Total	100.01	99.98	100.00	100.00	100.00	99.99	100.00

TABLE 1

CHEMICAL ANALYSES OF SAMPLES USED IN ESTIMATION OF HEAT CAPACITY (Concluded)

Constituent	G4-1171.8	G4-1220.9	G4-1294	G4-1307.2A	G4-1307.2F	G4-1444.7	G4-1649.5
			Original Analyses* (wt%)				
SiO_2	75.16	75.32	75.39	75.78	76.20	65.43	68.20
TiO_2	0.11	0.11	0.12	0.11	0.11	0.11	0.08
Al_2O_3	12.89	12.96	12.74	12.86	12.85	11.93	11.54
Fe_2O_3	0.92	0.87	0.69	0.80	0.75	1.02	0.75
FeO	0.06	0.08	0.24	0.14	0.14	0.02	0.02
MnO	0.78	0.08	0.08	0.08	0.08	0.08	0.05
MgO	0.14	0.15	0.10	0.10	0.08	0.04	0.03
CaO	0.54	0.56	0.56	0.55	0.56	1.23	0.75
Na_2O	3.35	3.34	3.60	3.50	3.62	2.44	2.68
K_2O	4.70	4.80	4.64	4.80	4.66	4.36	4.44
P_2O_5	0.01	0.01	0.01	0.01	0.01	0.01	0.01
H_2O^+	0.68	0.61	0.98	0.60	0.40	8.21	6.82
H_2O^-	0.42	0.44	0.39	0.39	0.21	5.71	4.74
Total	99.76	99.33	99.55	99.72	99.68	100.58	100.12
			Normalized Analyses (wt%)				
SiO_2	75.66	76.17	76.03	76.29	76.61	68.97	71.51
TiO_2	0.11	0.11	0.12	0.11	0.11	0.11	0.09
Al_2O_3	12.98	13.11	12.85	12.95	12.92	12.57	12.10
Fe_2O_3	0.93	0.88	0.70	0.81	0.75	1.08	0.79
FeO	0.06	0.08	0.24	0.14	0.14	0.02	0.02
MnO	0.78	0.08	0.08	0.08	0.08	0.09	0.05
MgO	0.14	0.15	0.10	0.10	0.08	0.04	0.03
CaO	0.55	0.57	0.56	0.55	0.56	1.30	0.79
Na_2O	3.37	3.38	3.63	3.52	3.64	2.57	2.81
K_2O	4.73	4.85	4.68	4.83	4.68	4.60	4.66
P_2O_5	0.01	0.01	0.02	0.01	0.01	0.01	0.01
H_2O^+	0.68	0.62	0.99	0.60	0.40	8.65	7.15
Total	100.00	100.01	100.00	99.99	99.98	100.01	100.01

*From Connolly and Nimick (1990).

usefulness of the method was examined to the point of actually estimating heat capacities for the solid material. The decision not to make routine use of the mineral-summation method has been made for a number of reasons, as follows.

- Estimation of percentages of constituent phases is very difficult in some tuffaceous materials. This is especially true of zeolitic tuffs and tuffs that are partly vitric.

- Heat capacity data are not available for some volumetrically important phases, including clinoptilolite and clay.

- The heat capacity of a phase may vary with the composition of the phase (e.g., zeolites and clays) which may in turn vary significantly between, or even within, samples.

The use of quantitative x-ray diffraction, as described by Bish and Vaniman (1985) and Bish and Chipera (1986), would reduce the uncertainty in percentages of phases. Microprobe analyses could be made to obtain compositions of phases. However, heat capacity data still would not be available, and the data-gathering process would be made more labor-intensive than justifiable, given that another estimation method is available. Thus, for the present, use of the mineral-summation method has been discontinued in favor of the oxide-summation method.

2.4 Heat-Capacity Estimation by the Oxide-Summation Method

2.4.1 Data for Rock-Forming Oxides

Table 2 summarizes the published coefficients (for use in Equation 1) for the relevant rock-forming oxides listed in Section 2.2. The heat capacities of the oxides are plotted in Figure 3 as a function of temperature. Note that SiO_2 is represented by quartz (for use in devitrified and zeolitic samples) and by silica glass (for vitric samples).

TABLE 2

HEAT CAPACITY COEFFICIENTS[a] FOR ROCK-FORMING OXIDES AND WATER

	A	B	C	D	E	F	G
SiO_2 (Quartz)[b]	0.74233	6.2834×10^{-4}	0.0	0.0	0.0	0.0	-1.6673×10^{4}
SiO_2 (Glass)[b]	1.2422	-1.2082×10^{-4}	0.0	9.2709×10^{-8}	0.0	0.0	-5.1767×10^{4}
TiO_2 [b]	0.78948	1.4152×10^{-4}	0.0	0.0	-0.070289	0.0	-1.2344×10^{4}
Al_2O_3 [b]	1.5048	1.9302×10^{-5}	0.0	0.0	-8.833	0.0	-1.9916×10^{4}
Fe_2O_3 [b]	-5.2514	-1.4674×10^{-2}	0.54182	3.796×10^{-6}	0.0	0.017422	0.0
FeO[b]	0.93876	5.2379×10^{-5}	0.0	0.0	-5.3197	0.0	4.4002×10^{3}
MnO[b]	0.84228	5.0749×10^{-5}	0.0	0.0	-3.9845	0.0	-4.4211×10^{2}
MgO[b]	1.618	-3.1508×10^{-5}	0.0	0.0	-9.608	0.0	-1.1459×10^{4}
CaO[b]	0.93479	6.5504×10^{-5}	0.0	0.0	-0.90922	0.0	-1.3386×10^{4}
Na_2O[b]	1.8388	1.2078×10^{-4}	0.0	0.0	-13.123	0.0	0.0
K_2O[b]	0.52301	4.8897×10^{-4}	0.0	0.0	6.5234	0.0	-1.4066×10^{4}
P_2O_5[b]	0.24686	1.5917×10^{-3}	0.0	0.0	0.0	0.0	0.0
H_2O (Hydrate)[c]	3.1592	0.0	0.0	0.0	-14.646	0.0	0.0
H_2O (Hydroxyl)[c]	7.5924	-7.0703×10^{-4}	0.0	0.0	-96.744	0.0	3.7165×10^{4}
H_2O (Structural)[d]	1.6513	1.9137×10^{-3}	0.0	0.0	0.0	0.0	0.0
H_2O (Perlitic)[e]	0.097545	8.6629×10^{-3}	0.0	0.0	0.0	0.0	0.0

[a]All coefficients are for a per-gram basis when combining heat capacities of more than one oxide. These coefficients are relevant to Equation 1.
[b]Converted from per-mole values in Robie et al. (1978).
[c]From Robinson and Haas (1983).
[d]From Helgeson et al. (1978).
[e]From King et al. (1948).

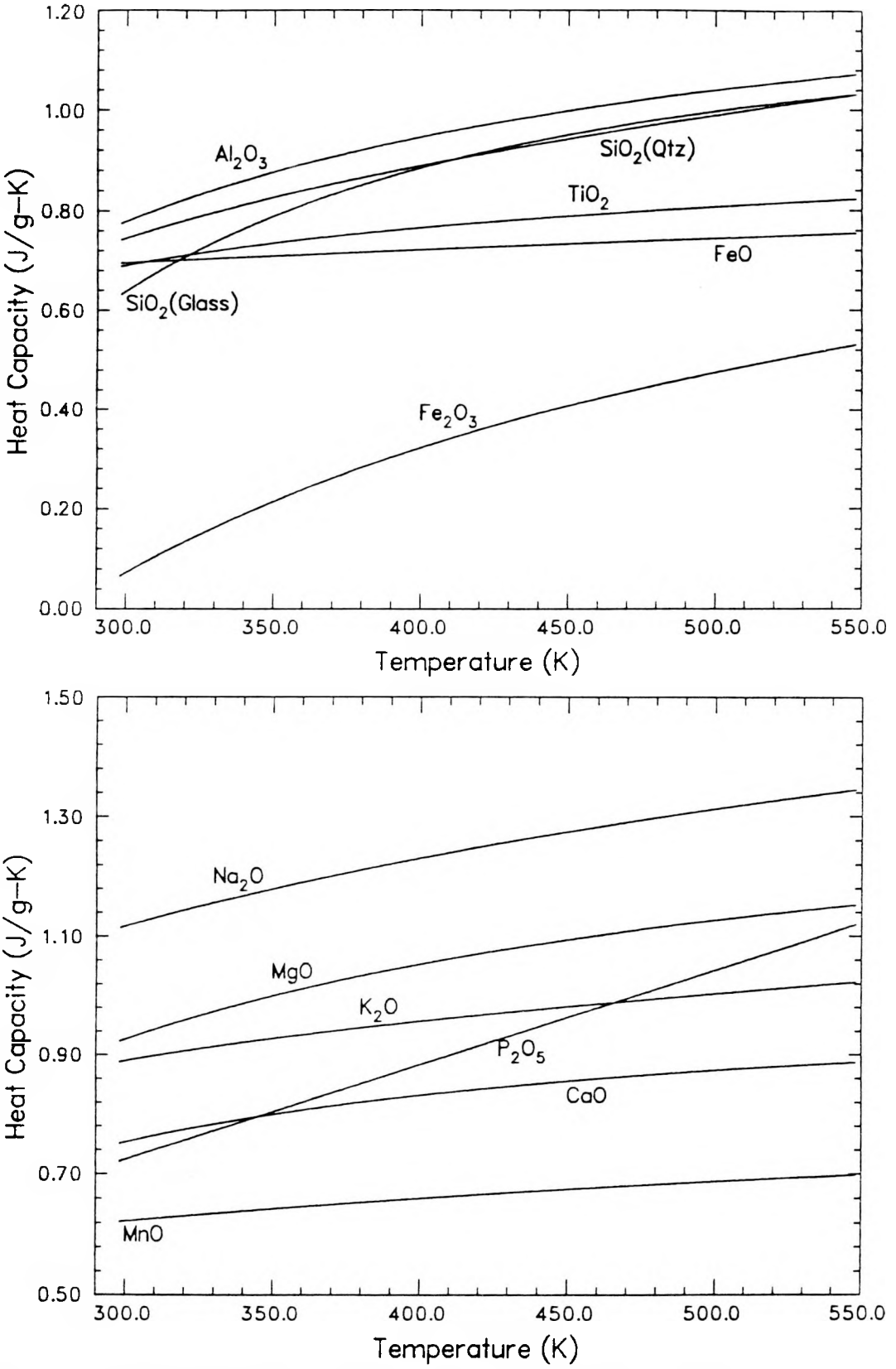

Figure 3. Heat Capacities of the Major Rock-Forming Oxides as a Function of Temperature

It should be noted here that devitrified samples are a compositionally distinct group, with mineralogy dominated by quartz, cristobalite, and feldspar and having a very low water content. Although zeolitized samples technically also are devitrified, the use of the term devitrified is reserved here for tuffs dominated by the mineral phases mentioned above. Also, note that the distinction between zeolitized and glassy samples is not always clear. Although petrographic and x-ray data for the samples used in this study (Connolly and Nimick, 1990) indicate that there is a clear distinction between these types in this group of samples, it is common for some glassy samples to be partly zeolitized and vice-versa.

2.4.2 Data for Water in Mineral Structures

Several heat capacity functions have been suggested for water that is bound within a mineral or glass structure. In the chemical analyses, all of this water is reported as H_2O^+, although it may be present in the structure of the material as molecular H_2O with various bond characteristics, or as the hydroxyl ion (OH^-). The values of the coefficients used for the heat capacity equations are ultimately dependent on the characteristics of these bonds. The actual equations used here are derived from published literature. In most cases, the equations are based on experimental work done on samples for which some information about the bond characteristics is known. In the case of perlite, the equations are based on experimental data alone, without much insight into what the molecular bonding characteristics are.

Figure 4 shows the heat capacities as a function of temperature for the four different water equations considered here. Comparison with the curves for all the solid components (Figure 3) show that any of the possible heat capacities for water are greater than those for the rock-forming oxides. The choice of a particular function for the heat capacity of H_2O may significantly affect the resultant heat capacity for the material as a whole, with the magnitude of this effect increasing with the water content of the solid material.

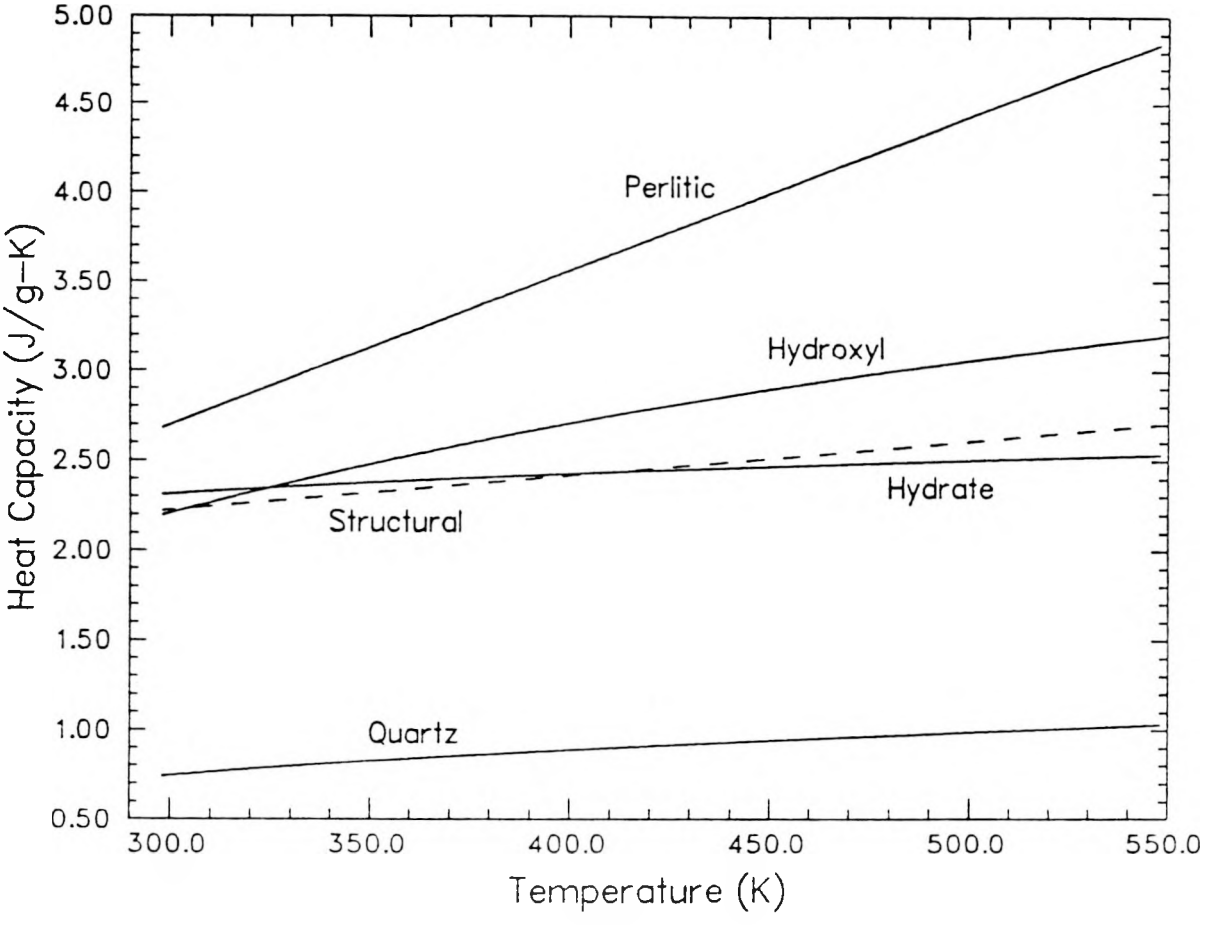

Figure 4. Heat Capacities of Four Types of Water (Quartz is included for comparison.)

The effect of these four different types of water bonds on the calculated heat capacity of solid material in a devitrified sample (Sample G1-1151.1) is shown in Figure 5. The choice of water bonding type makes little difference for devitrified samples even for those samples with relatively high H_2O^+ content (Sample G1-1511.1 contains 0.90 wt% H_2O^+).

The heat capacity curve for perlitic water was derived from the heat capacity function of King et al. (1948). These data were derived from dehydration and heat-of-solution experiments performed on samples of perlite (H_2O content 3.3 wt%), and are applied here only to perlitic glass samples.

The three remaining heat capacity functions for water which may be used are "hydroxyl," "hydrate" (both from Robinson and Haas, 1983), and "structural" (Helgeson et al., 1978). Helgeson's equation is derived from high-temperature calorimetric data reported by Pankratz (1964) for muscovite and dehydrated muscovite. The derivation of the "hydrate" equation of Robinson and Haas (1983) is inferred to be from simultaneous evaluation and correlation of thermodynamic data derived from experimental data on hydroxyl-bearing minerals (muscovite, anthophyllite, brucite, kaolinite, gibbsite, talc, etc.) using the computer code described by Haas (1974) and Haas and Fisher (1976). The "hydroxyl" equation of Robinson and Haas (1983) appears to have been similarly derived using heat capacity data for mineral phases containing bound molecular water (analcite, magnesium hydroxide, etc.). Although both equations appparently represent data from OH^--bearing minerals, "hydroxyl" and "structural" curves are notably different, whereas the "hydrate" and "structural" curves are very similar. The quality of these equations cannot be evaluated without experimental data.

Mineralogic data in Bish and Vaniman (1985) and Bish and Chipera (1986) indicate that the major hydrous phase in Units TSw1 and TSw2 is smectite clay. Additional OH^- should be present in biotite and hydrated iron oxides, and some hydrate water may be contained in ubiquitous cristobalite (and local tridymite) in these units. For the purposes of

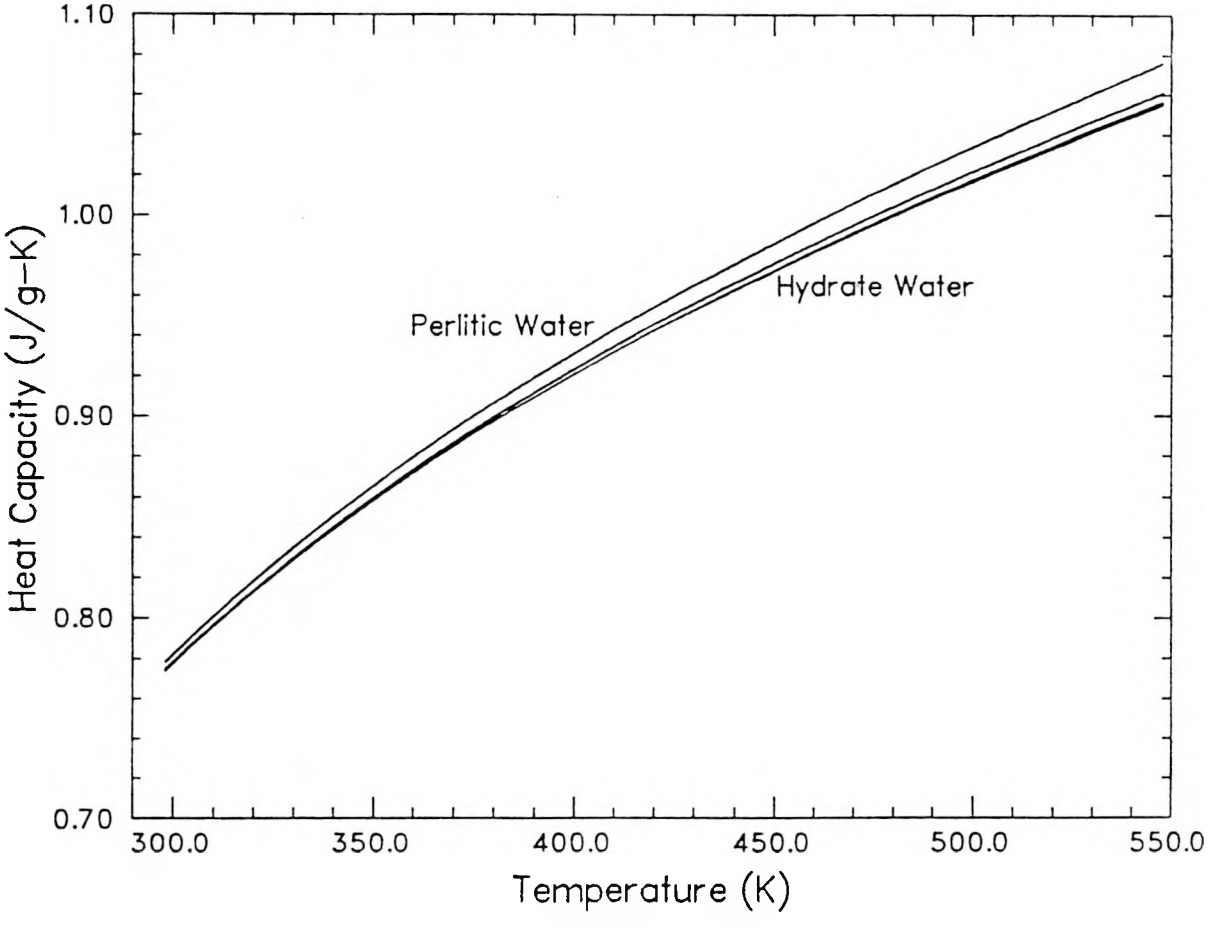

Figure 5. Heat Capacity of a Devitrified Sample (Sample G1-1151.1) Calculated Using Each of the Four Types of H_2O^+

this preliminary modeling work, "hydroxyl" is selected as the best choice for H_2O when calculating the heat capacity of devitrified samples.

Figure 6 shows the heat capacity of Sample G4-1444.7, a zeolitized sample, calculated for each of the four kinds of water. (As with Sample G1-1151.1, this sample was selected because it contains the highest H_2O^+ content of all samples of the lithology which it represents.) Because of the higher H_2O^+ content in zeolitized samples, the range of heat capacities caused by the different types of water is larger than the range in devitrified samples.

Helgeson et al. (1978), based on interpretations of published data, suggested that the heat capacity of H_2O in zeolites was essentially constant at temperatures above 298.15°K. Helgeson's plots of the data for analcime and dehydrated analcime at temperatures less than 298.15°K from King (1955) and King and Weller (1961) (Helgeson's Figure 14) do not show the parallelism which would support this suggestion, and nothing in the higher temperature data for dehydrated analcime (Pankratz, 1968) supports this suggestion. Dehydration studies by Knowlton and McKague (1976) and Knowlton et al. (1981) show a temperature dependence in the effective heat capacity of zeolitic water. For these reasons, a constant heat capacity value for zeolitic water is not considered reasonable for these whole-rock modeling studies.

As mentioned earlier in this section, heat capacity data for perlitic water were derived specifically for use with vitric material (and is used for vitric samples in this study). Although some zeolitic samples do contain glassy, perlitic material, the relative amounts of perlitic water have not been quantified and would be difficult to estimate. Thus, for the purposes of this preliminary modeling, the equation for perlitic water is not used for zeolitic samples. The validity of this approach must be checked when heat capacity data are obtained from experiments.

Knowlton et al. (1981) report data from TGA of twelve clinoptilolite-bearing tuffs that provide the following estimates of proportions of loosely-bound and tightly-bound water:

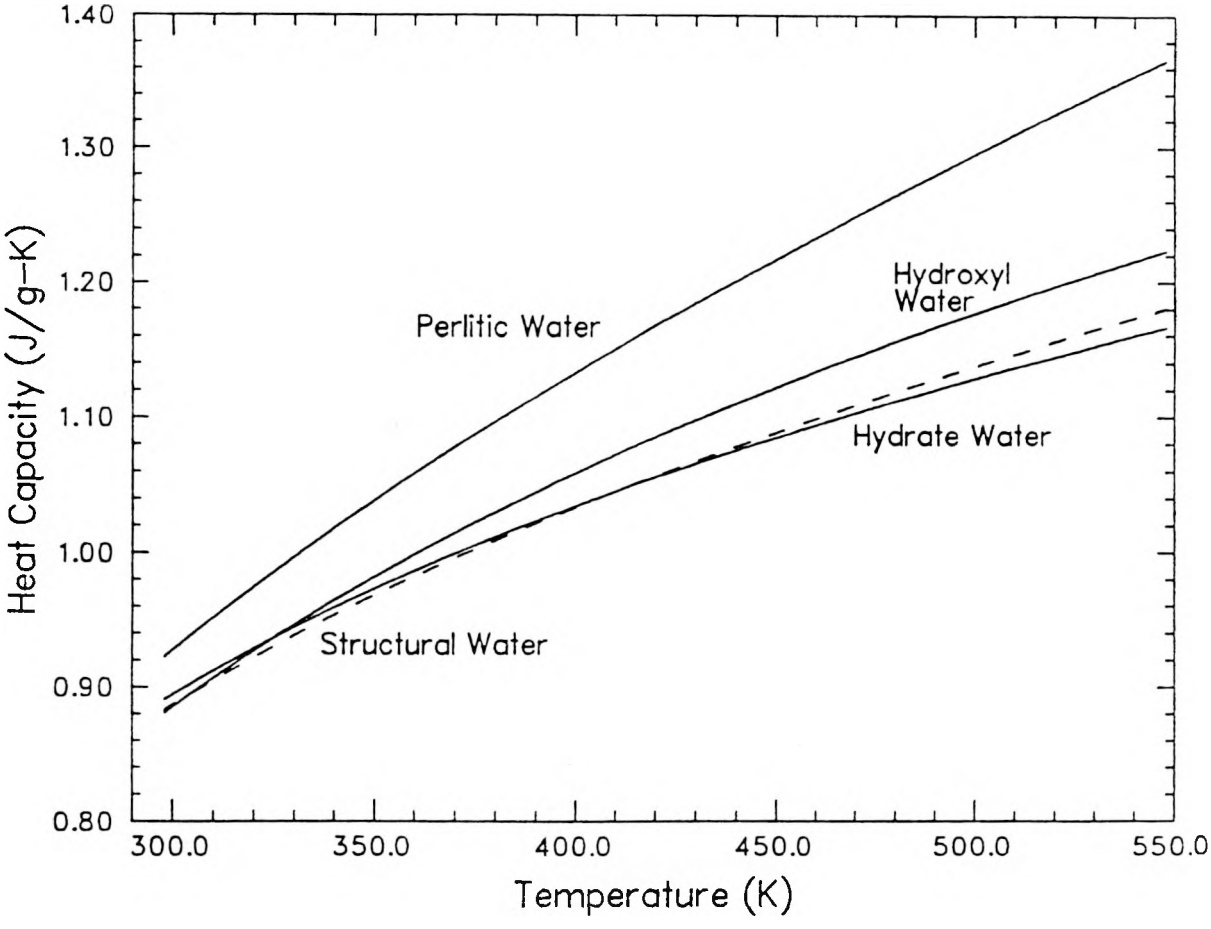

Figure 6. Heat Capacity of a Zeolitized Sample (Sample G4-1444.7) Calculated Using the Four Types of H_2O^+

Loosely-bound = 70%

Tightly-bound = 30%

where the values are percentages of the amount of H_2O^+ present. These proportions are used in the remainder of this paper to estimate heat capacities for zeolitic tuffs, with "loosely-bound" water taken to be hydrate water and "tightly-bound" water taken to be hydroxyl water.

2.5 Heat Capacities of Solids

2.5.1 Devitrified Samples

The bulk chemistries of twelve devitrified samples of the Topopah Spring Member in Table 1 have been used with Equations 1 and 2 to calculate the heat capacities of the solid portion of the samples. The results are shown in Figures 7a and 7b. There is very little variability in the estimated heat capacities, so the bulk-chemistry data for all twelve samples have been averaged (Table 3) and a single heat capacity equation as a function of temperature has been obtained using the resulting compositions and Equations 1 and 2. The equation is as follows:

$$C_p = 0.8586 + 3.4954 \times 10^{-4}\, T + 5.5807 \times 10^{-3}\, T^{1/2} + 3.9099 \times 10^{-8}\, T^2$$

$$- 1.9925\, T^{-1/2} + 1.7945 \times 10^{-4}\, T^{-1} - 1.5786 \times 10^{4}\, T^{-2} \quad . \qquad (3)$$

The curve described by Equation 3 is the baseline portion of the curve plotted in Figure 8.

Two of the SiO_2 phases that occur in the devitrified portion of the Topopah Spring Member--tridymite and cristobalite--undergo polymorphic transformations within the temperature range of interest here (25 to 275°C). These transformations absorb heat, so that the effective heat capacity of the solid material containing these two phases is higher than that calculated from bulk chemistry for temperatures at which the transformations occur. The derivation of the heat capacities of the transformations is described in the following paragraphs.

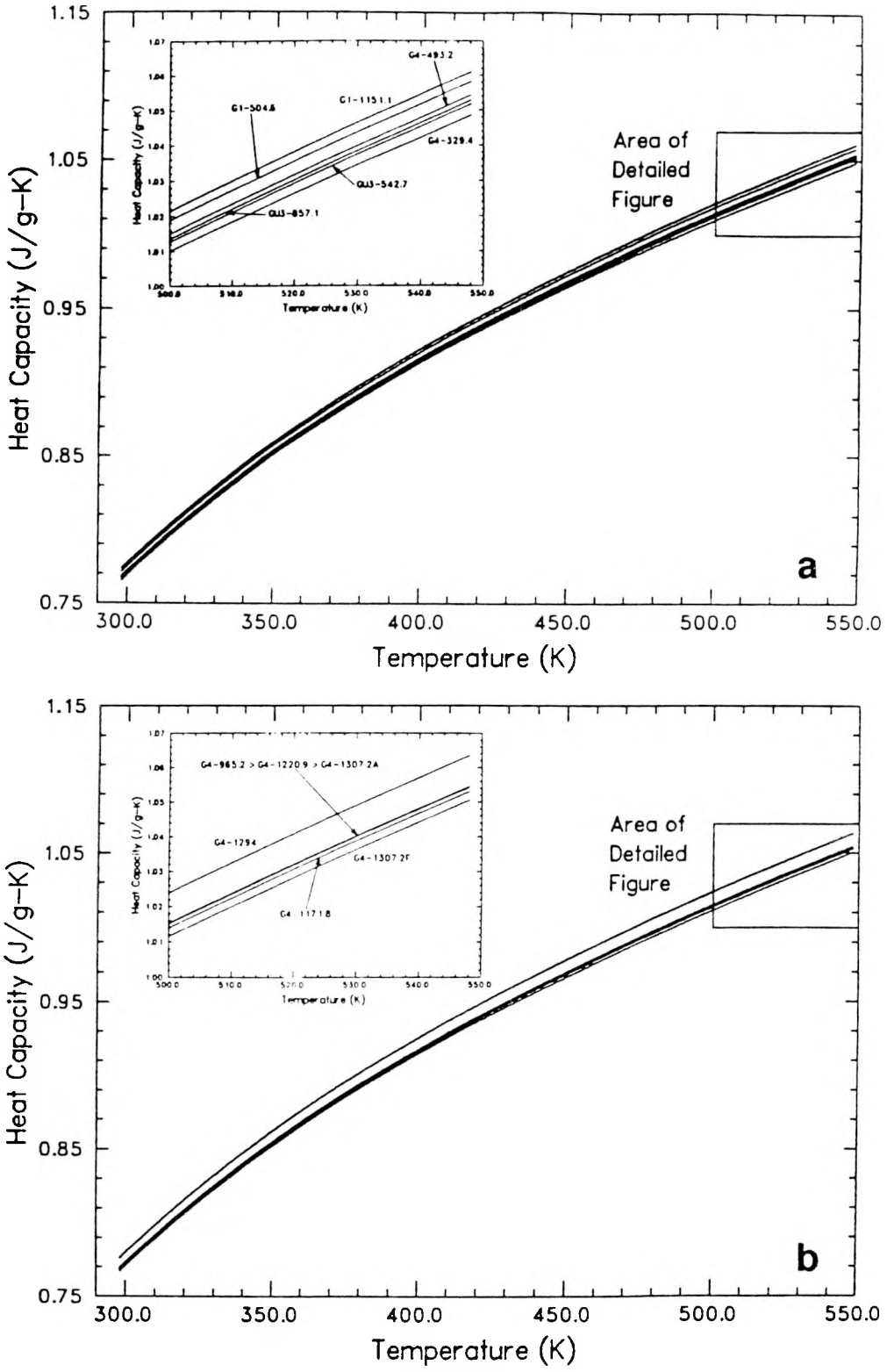

Figure 7. Heat Capacities of Twelve Devitrified Samples of the Topopah Spring Member [The sample group has been divided into two separate figures (a and b) for clarity only.]

TABLE 3

AVERAGE[a] CHEMICAL COMPOSITION FOR DEVITRIFIED SAMPLES

Constituent	Amount (wt%) Mean Value	St. Dev.[b]
SiO_2	75.35	2.09
TiO_2	0.15	0.09
Al_2O_3	13.38	0.94
Fe_2O_3	1.03	0.37
FeO	0.06	0.08
MnO	0.14	0.20
MgO	0.15	0.06
CaO	0.60	0.15
Na_2O	3.54	0.32
K_2O	4.93	0.34
P_2O_5	0.02	0.02
H_2O^+	0.66	0.18
Total	100.00	

[a]Averages of normalized analyses for the following 12 samples from Table 1: G1-504.6, G1-1151.1, GU3-542.7, GU3-857.1, G4-329.4, G4-493.2, G4-965.2, G4-1171.8, G4-1220.9, G4-1294, G4-1307.2A, G4-1307.2F.
[b]Calculated with n-1 degrees of freedom.

The tridymite transformation of interest here occurs at 163°C in the pure phase. However, this temperature may vary depending on the microstructural environment of the tridymite crystals, chemical impurities in the tridymite, or both (Sosman, 1965). Thermal expansion data for samples of the devitrified portion of the Topopah Spring Member (Nimick and Schwartz, 1987) suggest that tridymite in this material does indeed transform over a temperature interval. For the heat capacity calculations, the temperature interval is arbitrarily assumed to be 20°C, centered on 163°C. (This assumption is discussed in more detail in Section 4.5.1.)

The heat involved in the transformation depends on the amount of tridymite present and on the heat of transformation. Mineralogic data reported by Bish and Vaniman (1985) and Bish and Chipera (1986) have been used to obtain an average tridymite content of 3.56 wt% for Unit TSw2.

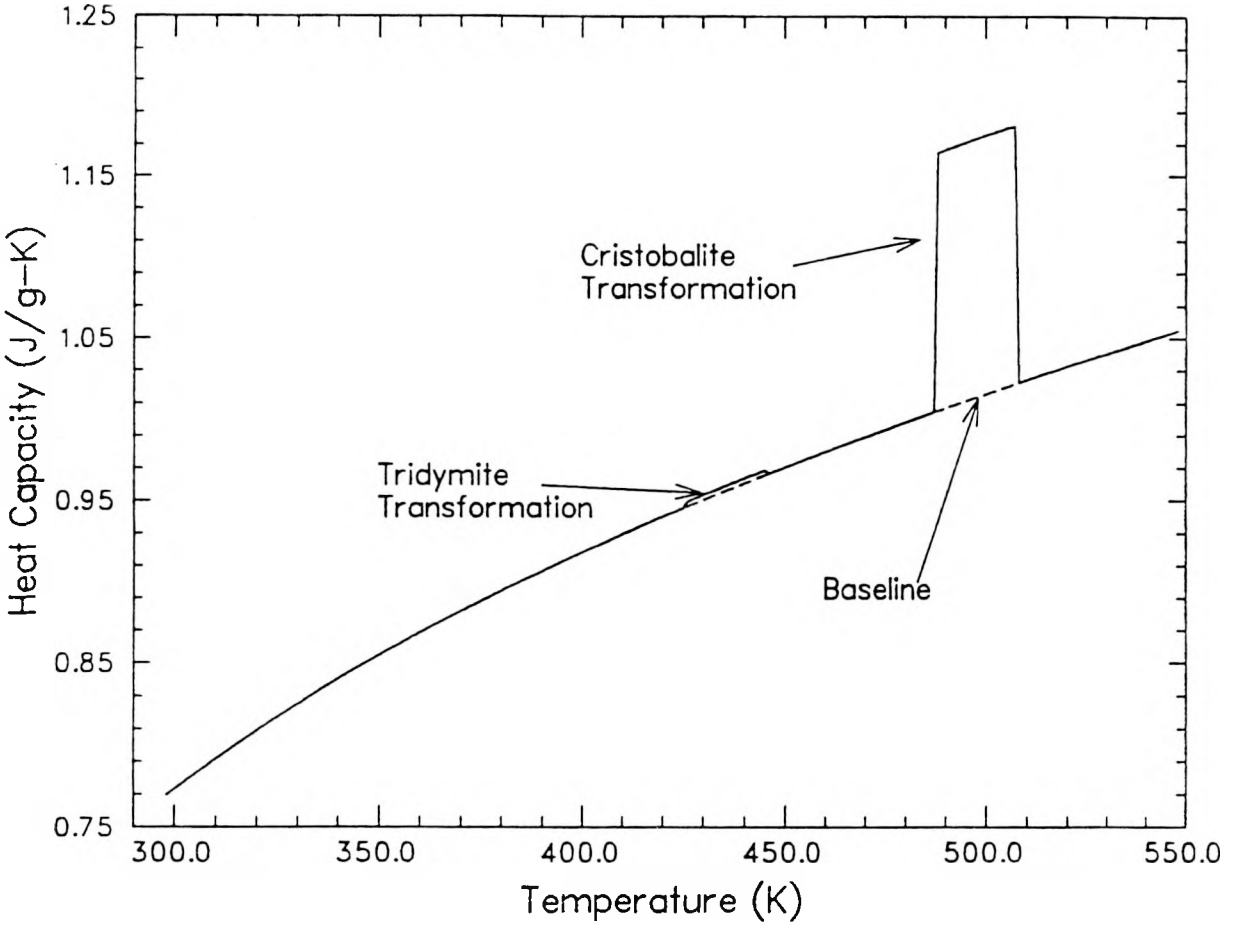

Figure 8. Average Heat Capacity for the Devitrified Portion of the Topopah Spring Member, Including Tridymite and Cristobalite Transformations

Shahid and Glasser (1970) report a value of 100.4 J/mole for the tridymite transformation at 163°C. Assuming that this heat is absorbed uniformly over the 20°C interval, the following additive "heat capacity" is calculated for each temperature in the interval:

$$\Delta C_{p,trid} = (100.4 \text{ J/mole})\left(\frac{1 \text{ mole}}{60.0888 \text{ g}}\right)\left(\frac{1}{20 \text{ K}}\right)(0.0356)$$

$$= 0.0030 \text{ J/g-K} \quad . \tag{4}$$

A similar discussion applies for cristobalite. The transformation interval again is assumed to be 20°C wide, centered on 225°C. The heat of transformation is given by Robie et al. (1978) as 1343 J/mole, and the mineralogic data of Bish and Vaniman (1985) and Bish and Chipera (1986) indicate an average cristobalite content of 14.27 wt% for Unit TSw2. Thus,

$$\Delta C_{p,crist} = (1343 \text{ J/mole})\left(\frac{1 \text{ mole}}{60.0888 \text{ g}}\right)\left(\frac{1}{20 \text{ K}}\right)(0.1427)$$

$$= 0.1595 \text{ J/g-K} \quad . \tag{5}$$

The additive effects of the tridymite and cristobalite transformations are shown in Figure 8. Obviously, the resulting curve for the heat capacity of the devitrified portion of the Topopah Spring Member (Figure 8) is simplistic. The amounts of tridymite and cristobalite will vary from sample to sample, and the temperature intervals of the transformations may be either narrower or wider than those assumed here. Also, the heat of transformation may not be uniformly distributed over the relevant temperature intervals. Nevertheless, the average amount of <u>total</u> heat involved in the transformations is believed to be a good estimate of the value that would be found in the actual rock, and the mean temperatures of the transformations should be correct. All of the assumptions made here will be examined during direct heat capacity measurements to be conducted in the future.

2.5.2 Vitric Samples

The bulk chemistries (Table 1) of three samples of the basal vitrophyre of the Topopah Spring Member have been used with Equations 1 and 2 to calculate the heat capacities of the solid portion of the samples. The results are shown in Figure 9. The bulk-chemistry data have been averaged (Table 4), then the compositional information has been used with Equations 1 and 2 to yield the following heat capacity equation for solid vitric material as a function of temperature:

$$C_p = 1.1745 + 1.8813 \times 10^{-4}\, T + 3.4676 \times 10^{-3}\, T^{1/2} + 9.2565 \times 10^{-8}\, T^2 - 1.3223\, T^{-1/2} + 1.115 \times 10^{-4}\, T^{-1} - 4.1386 \times 10^{4}\, T^{-2} \quad . \qquad (6)$$

2.5.3 Zeolitized Samples

The bulk chemistries (Table 1) of five zeolitized samples have been used with Equations 1 and 2 to calculate the heat capacities of the solid portion of the samples. The results are shown in Figure 10. In addition, the bulk-chemistry data have been averaged (Table 5), then the compositional information has been used with Equations 1 and 2 to yield the following heat capacity equation as a function of temperature:

$$C_p = 1.0366 + 2.7015 \times 10^{-4}\, T + 6.9353 \times 10^{-3}\, T^{1/2} + 4.8589 \times 10^{-8}\, T^2 - 3.8365\, T^{-1/2} + 2.23 \times 10^{-4}\, T^{-1} - 1.4391 \times 10^{4}\, T^{-2} \quad . \qquad (7)$$

The five curves shown in Figure 10 are dashed lines for temperatures above 95°C (368 K) because zeolites begin to dehydrate when the adjacent environment is dry, which would be the case in a porous material when pore water boils away at ambient temperature. The dashed lines represent the data calculated using Equation 7 and assuming that no zeolite dehydration occurs.

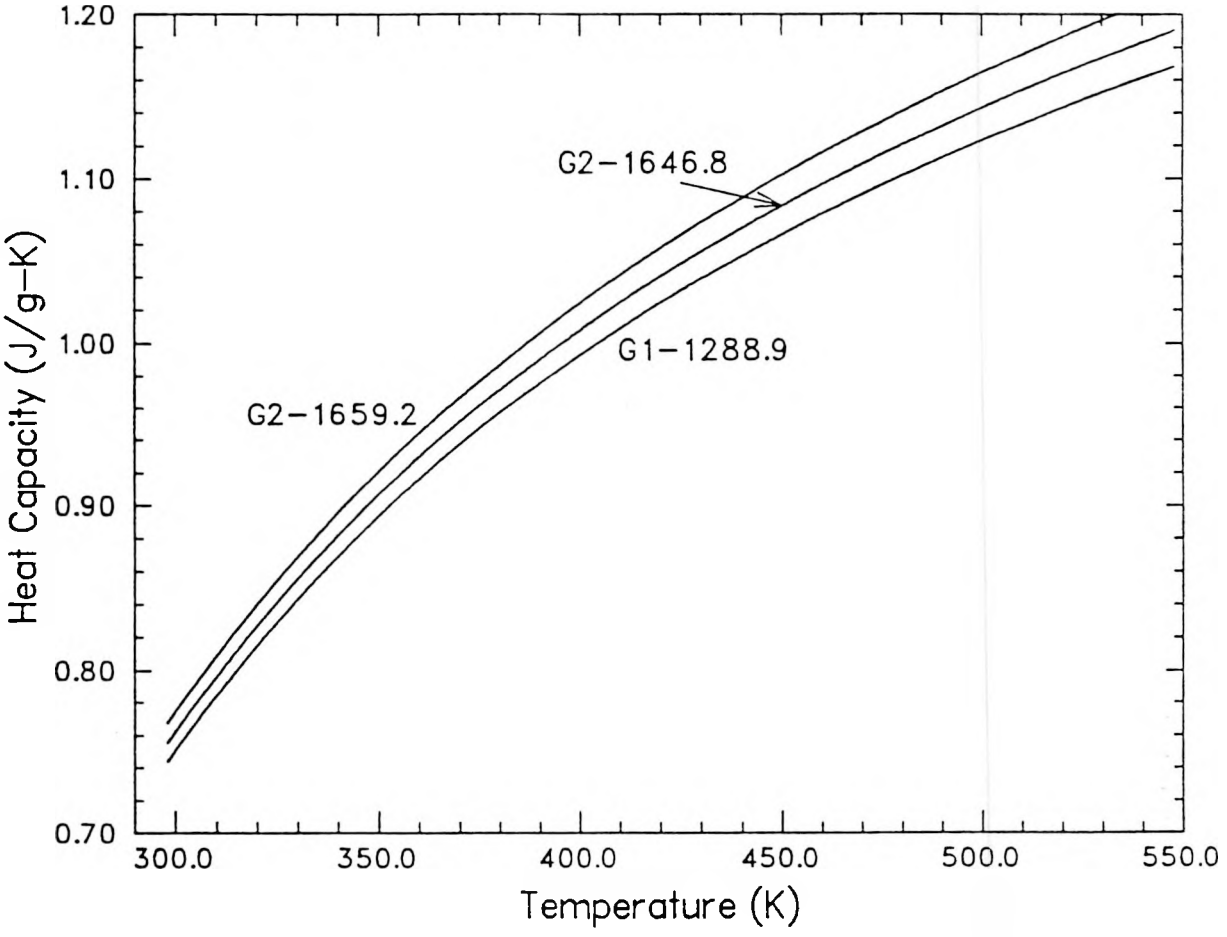

Figure 9. Heat Capacities of Solid Material for Three Samples of the Basal Vitrophyre of the Topopah Spring Member

TABLE 4

AVERAGE[a] CHEMICAL COMPOSITION FOR VITRIC SAMPLES

Constituent	Amount (wt%) Mean Value	St. Dev.[b]
SiO_2	73.65	0.71
TiO_2	0.11	0.00
Al_2O_3	12.80	0.06
Fe_2O_3	0.64	0.05
FeO	0.25	0.09
MnO	0.08	0.00
MgO	0.06	0.01
CaO	0.69	0.17
Na_2O	3.40	0.67
K_2O	4.37	0.61
P_2O_5	0.01	0.00
H_2O^+	3.95	0.67
Total	100.01	

[a]Averages of normalized analyses for the following three samples from Table 1: G1-1288.9, G2-1646.8, and G2-1659.2.
[b]Calculated with n-1 degrees of freedom.

A more realistic representation of the temperature dependence of the heat capacity of zeolitized material is obtained if zeolite dehydration is included. Data from Knowlton et al. (1981) were cited earlier in the discussion of the types of water in zeolitized tuff. These researchers distinguished between loosely-bound (or hydrate) water and tightly-bound (or hydroxyl) water based on TGA results for samples of zeolitized tuff. Water loss was continuous during their experiments, indicating overlap of the temperature ranges for loss of different types of water. For simplicity, hydrate water is assumed to be the water lost between the onset of dehydration and 230°C; hydroxyl water is assumed to remain in the structure until much higher temperatures are reached. (Selection of 230°C as the upper temperature for loss of hydrate water is based on data in Knowlton and McKague, 1976.)

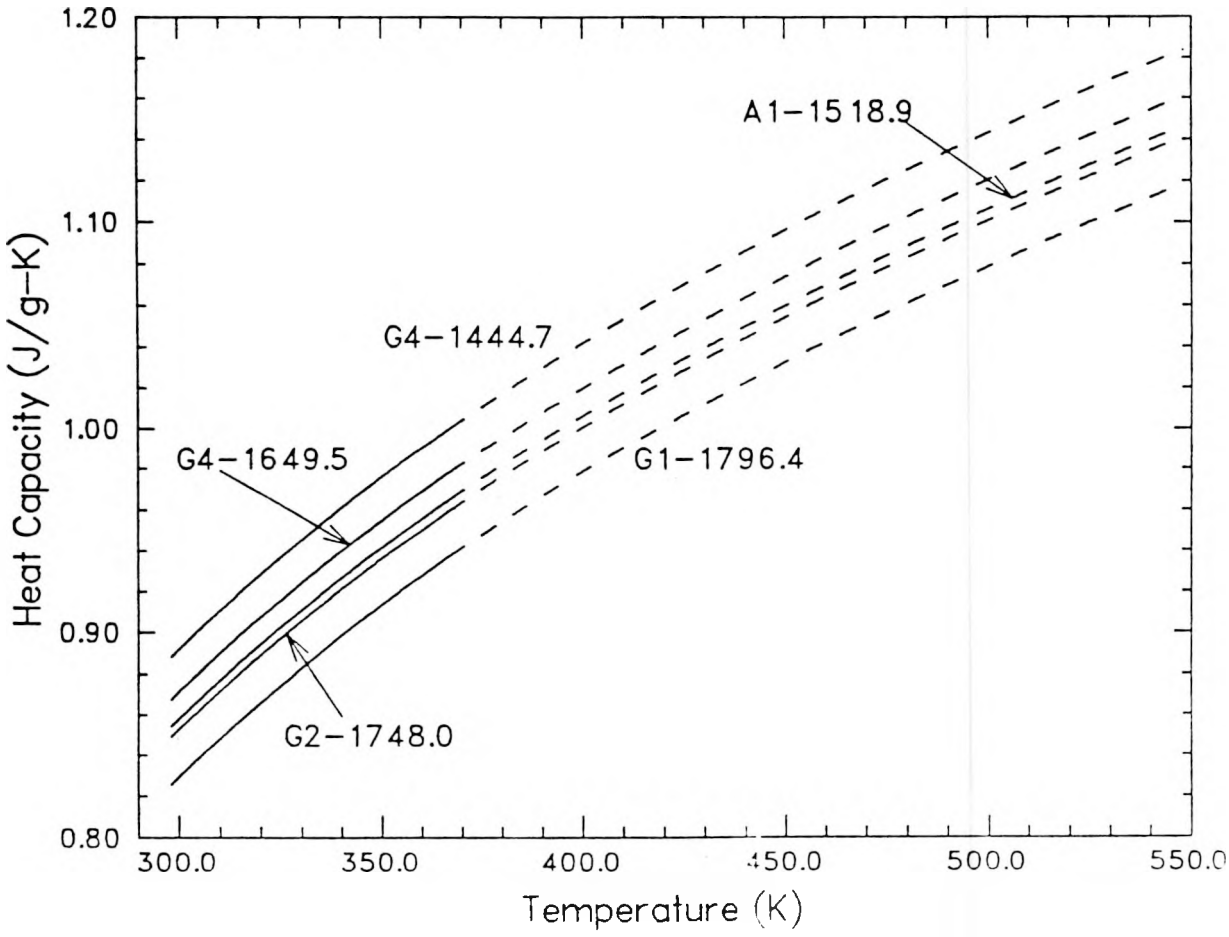

Figure 10. Heat Capacities of Solid Material for Five Zeolitized Samples from the Lower Topopah Spring Member and the Tuffaceous Beds of Calico Hills

TABLE 5

AVERAGE[a] CHEMICAL COMPOSITION FOR ZEOLITIZED SAMPLES

Constituent	Amount (wt%) Mean Value	St. Dev.[b]
SiO_2	70.80	2.76
TiO_2	0.14	0.11
Al_2O_3	12.51	1.24
Fe_2O_3	1.28	0.95
FeO	0.01	0.01
MnO	0.11	0.09
MgO	0.22	0.40
CaO	1.56	0.54
Na_2O	2.27	0.68
K_2O	4.26	0.41
P_2O_5	0.02	0.02
H_2O^+	6.81	1.23
Total	99.99	

[a]Averages of normalized analyses for the following five samples from Table 1: A1-1518.9, G1-1796.4, G2-1748.0, G4-1444.7, and G4-1649.5.
[b]Calculated with n-1 degrees of freedom.

This information has been used to calculate a change in heat capacity by assuming that the fraction of the water in the sample is a linear function of temperature between the temperature at the initiation of dehydration (assumed to be 95°C, as explained in Section 3.4) and 230°C. Assuming the fraction is 1.0 at 95°C and 0.3 at 230°C, the resulting equation is

$$x_{H_2O} = -0.0051852\ T + 2.9089259 \quad , \tag{8}$$

where x_{H_2O} is the fraction of the original amount of water (as H_2O^+) in the sample and T is absolute temperature. Figure 11 shows the heat capacity of the solid portion of Sample A1-1518.9 adjusted for this progressive dehydration of the zeolites.

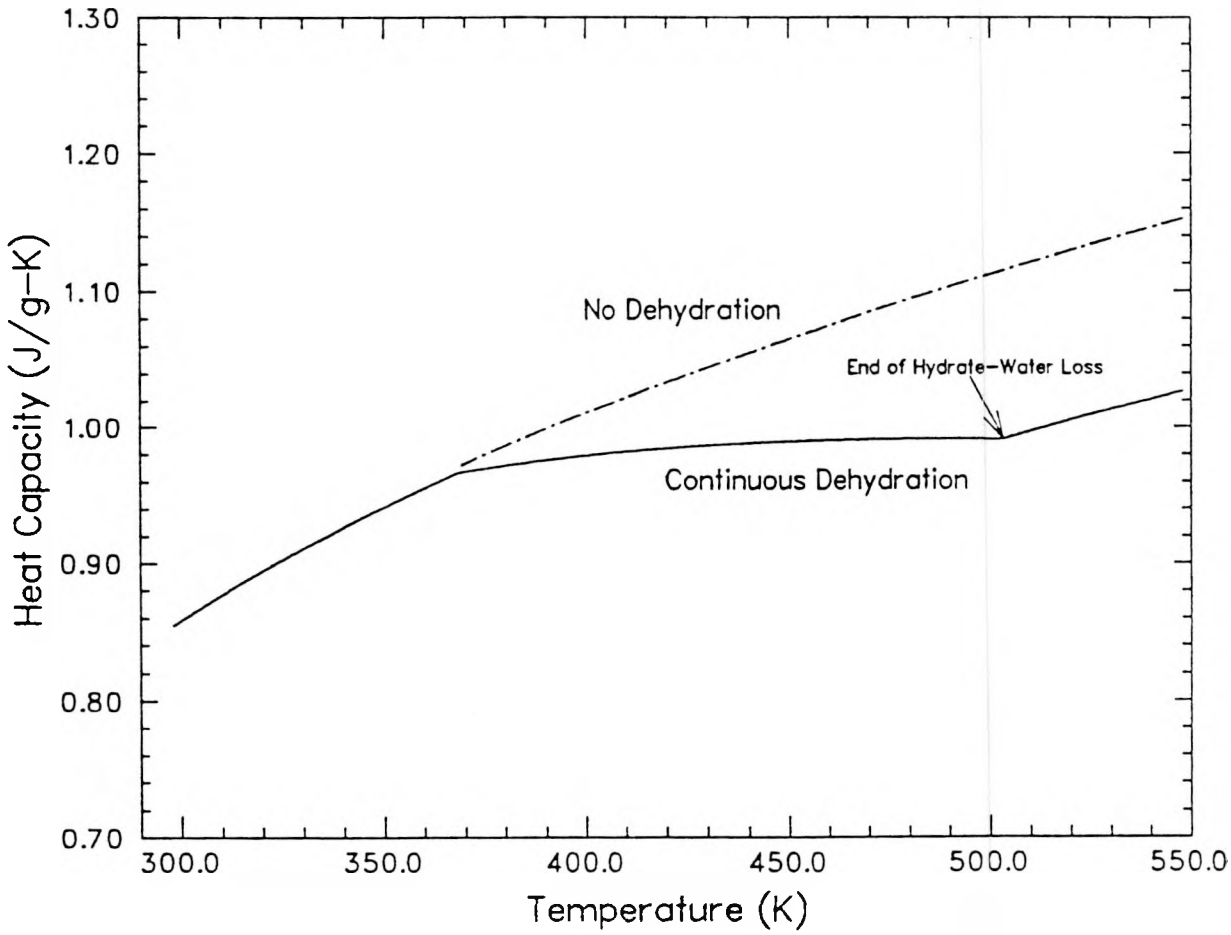

Figure 11. Comparison of Heat Capacities for Solid Material of a Zeolitized Sample With and Without Progressive Dehydration

3.0 THERMAL CAPACITANCE OF ROCK MASS

Once the heat capacities of solid components have been determined, the heat capacity and thermal capacitance (product of density and heat capacity) of the rock mass [$C_{p,rm}$ and $(\rho C_p)_{rm}$, respectively] are easily obtained. The relevant equations are

$$(\rho C_p)_{rm} = \rho_g (1 - \phi_m) (1 - \phi_L) C_{p,g} + (1 - \phi_L) \phi_m s\rho_w C_{p,w} + \left[\phi_L + (1 - \phi_L) \phi_m (1 - s)\right] \rho_a C_{p,a}$$

$$\approx \rho_g (1 - \phi_m) (1 - \phi_L) C_{p,g} + (1 - \phi_L) \phi_m s\rho_w C_{p,w} \quad , \qquad (9)$$

and

$$C_{p,rm} = \frac{(\rho C_p)_{rm}}{\rho_{rm}} \approx \frac{(\rho C_p)_{rm}}{\rho_g(1 - \phi_L) (1 - \phi_m) + (1 - \phi_L) \phi_m s\rho_w} \quad , \qquad (10)$$

where ϕ_m is matrix porosity,

ϕ_L is the volume fraction of lithophysal cavities,*

$C_{p,g}$ is the heat capacity of the solid portion of the rock,

s is the saturation of the matrix porosity,

$C_{p,w}$ and $C_{p,a}$ are the heat capacity of water and air, respectively,

ρ_g is grain density, and

ρ_w and ρ_a are the densities of water and air, respectively.

The simplification of Equations 9 and 10 results from the extremely low density of air; the products $[\phi_L + (1 - \phi_L)] \phi_m (1 - s)] \rho_a C_{p,a}$ and $[\phi_L + (1 - \phi_L) \phi_m (1 - s)] \rho_a$ are negligible relative to the first two terms in each equation.

---

*Lithophysal cavities are quite large relative to pores in the matrix. Because the matrix porosity is partially saturated, combined with the fact that larger voids fill with water later in the saturation process, the lithophysal cavities are assumed to be dry.

For this report, we have concentrated on the thermal capacitance because the most common requirement for heat capacity data is to solve heat-transfer problems in which the ratio of thermal conductivity to the thermal capacitance is the relevant property. Should data for the heat capacity of the rock mass be desired, Equation 10 can be used with the information in this report to calculate appropriate values.

An additional assumption implicit in Equations 9 and 10 is that fracture porosity (ϕ_f) does not contribute to $C_{p,rm}$ or $(\rho C_p)_{rm}$. Klavetter and Peters (1986) provide estimates of fracture porosity ranging from 1.3 to 18 x 10^{-5} for the units discussed in this report. Table 6 provides a comparison of the unit-specific values of fracture porosity and matrix porosity. Clearly, the fracture porosity will make a negligible contribution to calculation of values for $C_{p,rm}$ or $(\rho C_p)_{rm}$ using Equations 9 and 10.

3.1 Data for Grain Density, Matrix Porosity, Lithophysal-Cavity Abundance, and Saturation

3.1.1 Grain Density

Values used for grain density are given in Table 7. As noted in the table, the values for Units CHnlz and CHn2z are averages of data that analysis has shown to be spatially variable. For both units, the sparse data from USW G-1 indicate that the average grain density is higher in this core hole. If the data from USW G-1 are not included, thermal capacitances at 298.15 K would be lower by 1% or less.

3.1.2 Matrix Porosity

Matrix porosity values are listed in Table 6. As noted in the table, the value for Unit CHnlz is an average of data that analysis has shown to be spatially variable. The sparse data from USW G-1 indicate that the average matrix porosity of Unit CHnlz in this hole is higher than the matrix porosity in the unit in UE-25a#1 or USW G-4. If the data from USW G-1 are not included, the thermal capacitance at 298.15K for Unit CHnlz would be 0.3% lower.

TABLE 6

COMPARISON OF MATRIX AND FRACTURE POROSITIES

Thermal/Mechanical Unit	Matrix Porosity (ϕ_m)	Fracture Porosity[a] (ϕ_f)	$\frac{\phi_f}{\phi_m}$ (%)
TCw	0.107	1.4×10^{-4}	0.131
PTn	0.420[b]	2.7×10^{-5}	0.006
TSw1	0.154[c]	4.1×10^{-5}	0.027
TSw2	0.121	1.8×10^{-4}	0.149
TSw3	0.032[d]	4.3×10^{-5}	0.134
CHn1v	0.345[e]	4.6×10^{-5}	0.013
CHn2v	0.281	4.6×10^{-5}	0.016
CHn1z	0.328[f]	4.6×10^{-5}	0.014
CHn2z	0.216	4.6×10^{-5}	0.021

[a]Obtained from Table 2 of Klavetter and Peters (1986).
[b]Data from USW G-2 not used because of differences between material from USW G-2 and material from the proposed repository location.
[c]Data from all locations except USW G-2 have been combined despite the apparent spatial variability described by Rutherford and Nimick (in preparation).
[d]Data from UE-25a#1 have not been used because the values do not appear to be representative of the material.
[e]Data from USW G-4 have not been used because the values do not appear to be representative of the material.
[f]Data from all locations have been combined despite apparent spatial variability.

3.1.3 Lithophysal-Cavity Abundance

Lithophysal cavities occur only in the welded, devitrified units, as shown in Table 7. Cavity abundances have been measured only for the ash flows of the Topopah Spring Member (Spengler and Chornack, 1984), as summarized for Units TSw1 and TSw2 in Nimick and Schwartz (1987). The average abundance for Unit TSw1 has been assumed for Unit TCw because the description of the Tiva Canyon Member in Scott et al. (1983) suggests that lithophysal-cavity abundance in Unit TCw is relatively high.

TABLE 7

DATA FOR GRAIN DENSITY, LITHOPHYSAL-CAVITY ABUNDANCE, AND MATRIX SATURATION

Thermal/Mechanical Unit	Grain Density (g/cm^3)	Lithophysal-Cavity Abundance (volume fraction)	Matrix Saturation[a] (volume fraction)
TCw	2.50	0.045[b]	0.67
PTn	2.39[c]	-	0.61
TSw1	2.54	0.045[d]	0.65
TSw2	2.55	0.010[d]	0.65
TSw3	2.40	-	0.65
CHn1v	2.32	-	0.90
CHn2v	2.48	-	0.90
CHn1z	2.36[e]	-	0.91
CHn2z	2.44[e]	-	0.91

[a]Data taken from Montazer and Wilson (1984).
[b]Assumed to be the same as for Unit TSw1.
[c]Data from USW G-2 not used because of differences between material from USW G-2 and material from the proposed repository location.
[d]Data taken from Nimick and Schwartz (1987).
[e]Data from all locations combined despite apparent spatial variability.

3.1.4 Saturation

Saturation data have been taken from Montazer and Wilson (1984), as listed in Table 7. These values are assumed to apply only to matrix porosity, because lithophysal cavities and most fractures should be dry in materials that are not fully saturated.

Pore water has been assumed to boil over a 20°C range beginning at 95°C (Section 3.4). The saturation is assumed to decrease linearly from the initial value to zero over this temperature range. The relevant equation is

$$s = s_o\,(20.376316 - 0.05263T)\quad , \tag{11}$$

where s_o is the initial saturation and T is absolute temperature.

3.2 Data for Abundances of Cristobalite and Tridymite

Data for the abundances of cristobalite and tridymite in Units TCw, TSw1, and TSw2 were calculated from information in Bish and Vaniman (1985) for USW G-2, USW GU-3, and USW G-4 and in Bish and Chipera (1986) for UE-25a#1 and USW G-1. Data in these two reports were assigned to specific thermal/mechanical units based on information in Ortiz et al. (1985) and Nimick et al. (1988).

The mineralogic data are listed in the two source reports in one of two ways: (1) as a mean value plus and minus a standard deviation, or (2) as a range. For the purposes of this report, the mean values and the midpoints of the ranges were taken to be representative of mineralogy samples. These data were then combined to yield the mean values and standard deviations in Table 8.

The average values listed in Table 8 are the values used in the estimation of heat capacities. Mineralogic data from USW G-2 were not included in the averages because in each of the six cases the mean of the data from USW G-2 is significantly different than the means from the other four coreholes.

The averages for tridymite abundance in Units TCw and TSw2 are smaller than the associated standard deviations. This indicates that the assumption of a normal distribution for the data is erroneous. In fact, the data are dominated by very low values and are not normally distributed. However, the calculations of heat capacity are unaffected by this assumption because only the average abundances are used in the calculations.

3.3 Data for Density, Heat Capacity, and Enthalpy of Boiling of Water

The same procedure was used for each of the three properties of water used in the calculations of heat capacity. For a given property, data tabulated in handbooks as a function of temperature were used to obtain

TABLE 8

ABUNDANCES OF CRISTOBALITE AND TRIDYMITE

Abundances (Volume Percent)

Core Hole	Cristobalite Mean Value	Cristobalite Standard Deviation[a]	Tridymite Mean Value	Tridymite Standard Deviation[a]	No. of Samples
		Unit TCw			
UE-25a#1	24.33	0.56	0.00	0.00	3
USW G-1[b]	---	---	---	---	---
USW G-2	40.00	0.00	14.17	3.82	3
USW GU-3	20.11	7.77	4.61	8.18	9
USW G-4	29.33	2.31	0.00	0.00	3
Average, excluding USW G-2	22.80	7.05	2.77	6.61	15
		Unit TSw1			
UE-25a#1	13.83	5.19	4.18	3.90	6
USW G-1	12.20	9.15	11.20	7.73	5
USW G-2	25.28	7.75	3.61	5.74	9
USW GU-3	13.44	7.83	12.38	6.85	8
USW G-4	12.67	5.79	12.11	5.67	9
Average, excluding USW G-2	13.05	6.60	10.33	6.65	28
		Unit TSw2			
UE-25a#1	6.31	3.63	1.60	2.22	10
USW G-1	18.25	5.62	5.01	4.61	16
USW G-2	30.56	6.22	0.00	0.00	9
USW GU-3	15.05	6.89	1.91	3.48	11
USW G-4	14.85	6.20	4.69	6.36	13
Average, excluding USW G-2	14.27	7.04	3.56	4.71	50

[a]Standard deviation calculated for (n-1) degrees of freedom.
[b]Unit not present.

values at intermediate temperatures by linear interpolation. (Values of density and heat capacity at temperatures above 100°C were obtained by extrapolation of the linear segment between the highest two tabulated temperatures.)

It has been assumed that pore water will boil over a 20°C range in temperatures, beginning at 95°C (mentioned first in Section 3.1.4 and discussed in more detail in Section 3.4). In the calculations of heat capacity, the "heat capacity of boiling" has been calculated by estimating the enthalpy of boiling at a specific temperature, then dividing the enthalpy value by 20. The resulting value then was added to the calculated thermal capacitance at the relevant temperature.

In addition to boiling of pore water between 95 and 114°C, the amount of water released from zeolites in the zeolitized samples between 95 and 230°C also vaporizes. The heat absorbed for vaporization of these "packets" of water is added to the calculated thermal capacitance at each relevant temperature.

3.4 Boiling Temperature

The elevation at Yucca Mountain and, more specifically, at the level of the proposed repository, is high enough above sea level for the temperature at which water boils to be depressed from 100°C. Repository elevations range from 2935 to 3758.5 ft (894.6 to 1145.6 m) (DOE, 1987). Assuming that the boiling isotherm will extend as much as 200 m (656 ft) above and below the repository, based on Brandshaug (1991), the total range in elevations for which boiling may occur is estimated to be 2279 to 4415 ft (695 to 1345 m). Linear interpolation of air pressures from Bolz and Tuve (1973) yields an estimated pressure range of 0.08505 to 0.09203 MPa. Using these values and linear interpolation of pressure-temperature data for the vaporization curve of water (Bolz and Tuve, 1973), a range of 95.2 to 97.3°C is obtained for boiling temperatures for the pore water at Yucca Mountain. The lower value of 95°C has been adopted for the calculations of heat capacity.

Laboratory experiments involving temperature increases that reach and exceed the boiling point of water suggest that the pore water boils over a range of temperatures (e.g., Nimick, 1990). The width of this temperature range will depend on the hydrologic properties of the rock (i.e., the rate of water movement under a pressure gradient) and the rate of temperature increase. The range would become wider for more rapid heating, or in a rock with lower permeability. For the purposes of heat capacity estimation, a temperature range of 20°C has been arbitrarily selected.

3.5 Estimated Thermal Capacitances

The data described in the preceding portions of Section 3 have been combined with the heat capacity estimates for the solid material and Equation 9 to obtain estimates of the thermal capacitances of nine thermal/mechanical units. The results are provided in three forms. Table 9 lists values of thermal capacitance at a number of selected temperatures. Figures 12 through 14 show the thermal capacitances as continuous functions of temperature. Finally, the unit-specific forms of Equation 9 that were used to obtain the data in Table 9 and Figures 12 through 14 are listed in Appendix A.

TABLE 9

VALUES OF THERMAL CAPACITANCE* OF THE ROCK MASS
AT SELECTED TEMPERATURES FOR NINE THERMAL/MECHANICAL UNITS

	Thermal/Mechanical Unit								
T(°C)	TCw	PTn	TSw1	TSw2	TSw3	CHn1v	CHn2v	CHn1z	CHn2z
25	1.9263	2.1164	1.9779	2.0324	1.8443	2.4436	2.4030	2.6032	2.4588
50	2.0183	2.2196	2.0654	2.1280	2.0315	2.5557	2.5384	2.6647	2.5386
94	2.1494	2.3498	2.1891	2.2638	2.2831	2.6960	2.7121	2.7447	2.6484
95	9.6274	30.3260	12.6294	10.7683	4.5590	36.6013	30.3289	36.6069	25.6449
105	9.3665	29.2767	12.2534	10.4690	4.5188	35.3263	29.3015	35.3440	24.8091
114	9.1306	28.3302	11.9138	10.1984	4.4800	34.1764	28.3743	34.2053	24.0548
115	1.9278	1.3695	1.8555	2.0065	2.2953	1.5013	1.7617	2.7914	3.3671
155	2.0272	1.4612	1.9641	2.1114	2.4489	1.6018	1.8796	2.7419	3.3074
195	2.1053	1.5358	2.0264	2.1912	2.5740	1.6836	1.9756	2.6707	3.2214
235	2.1802	1.5986	2.0985	2.2692	2.6792	1.7525	2.0564	1.5814	1.9075
275	2.2492	1.6529	2.1649	2.3410	2.7702	1.8120	2.1262	1.6320	1.9685

*Units are J/cm^3K.

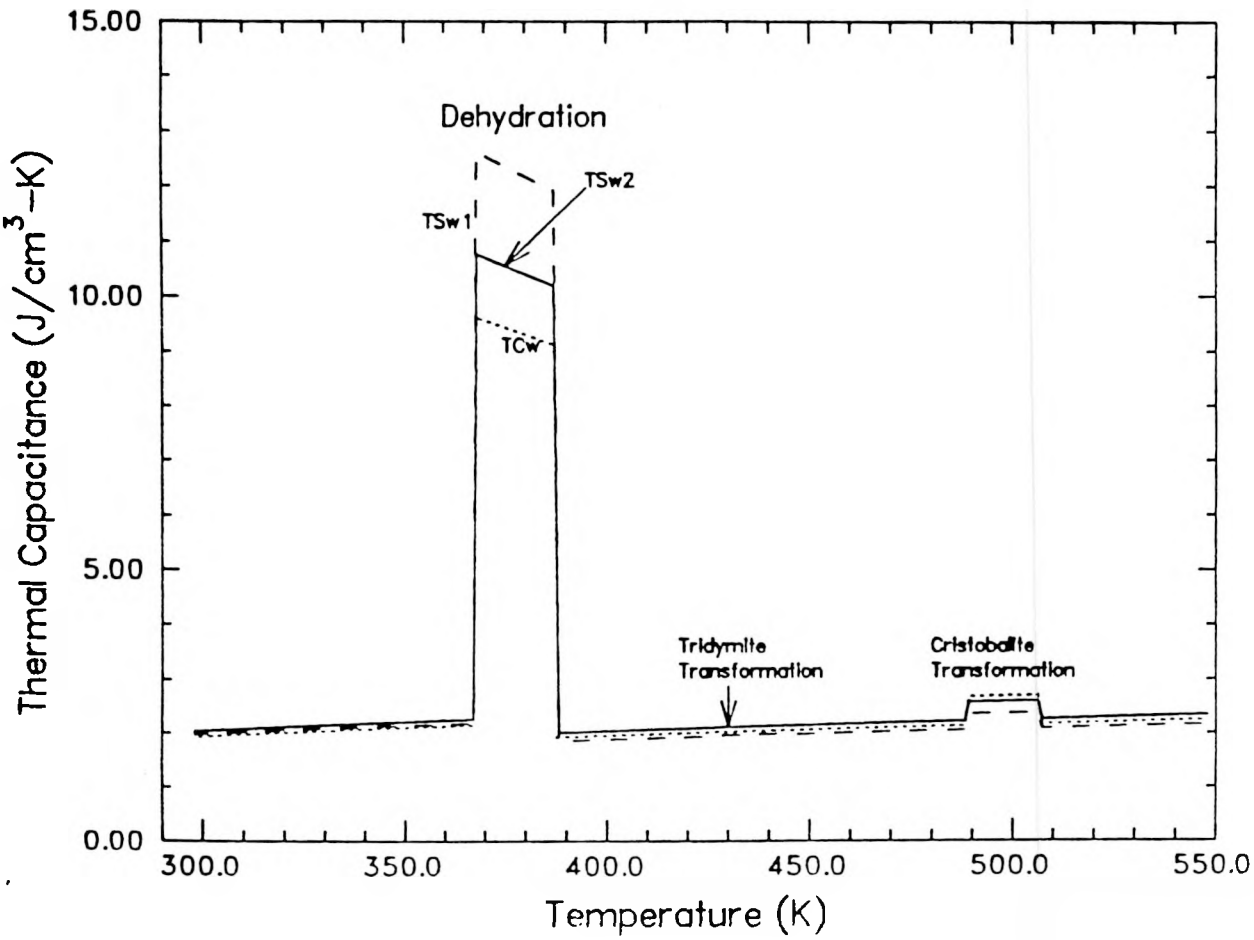

Figure 12. Rock-Mass Thermal Capacitances of Devitrified Units

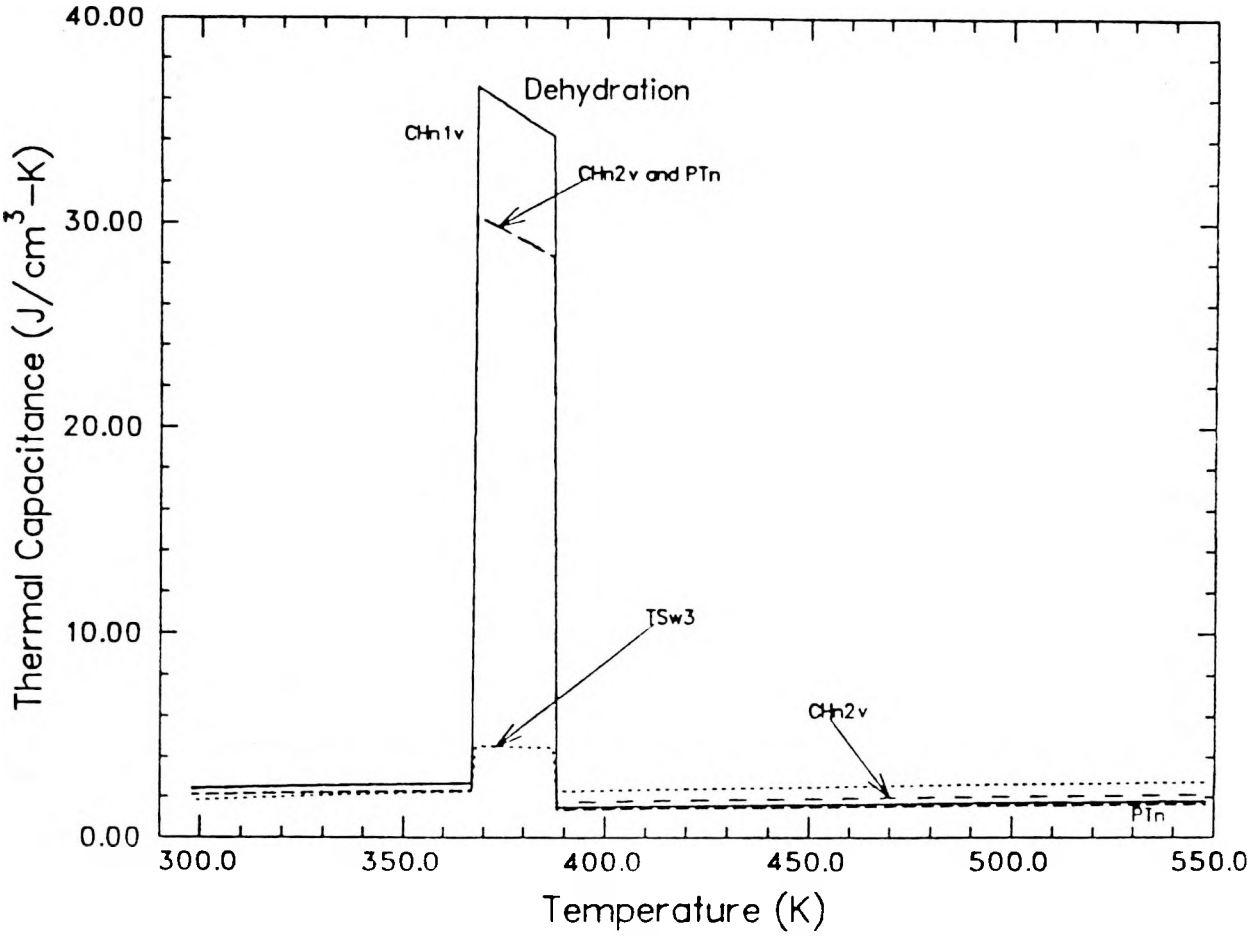

Figure 13. Rock-Mass Thermal Capacitances of Vitric Units

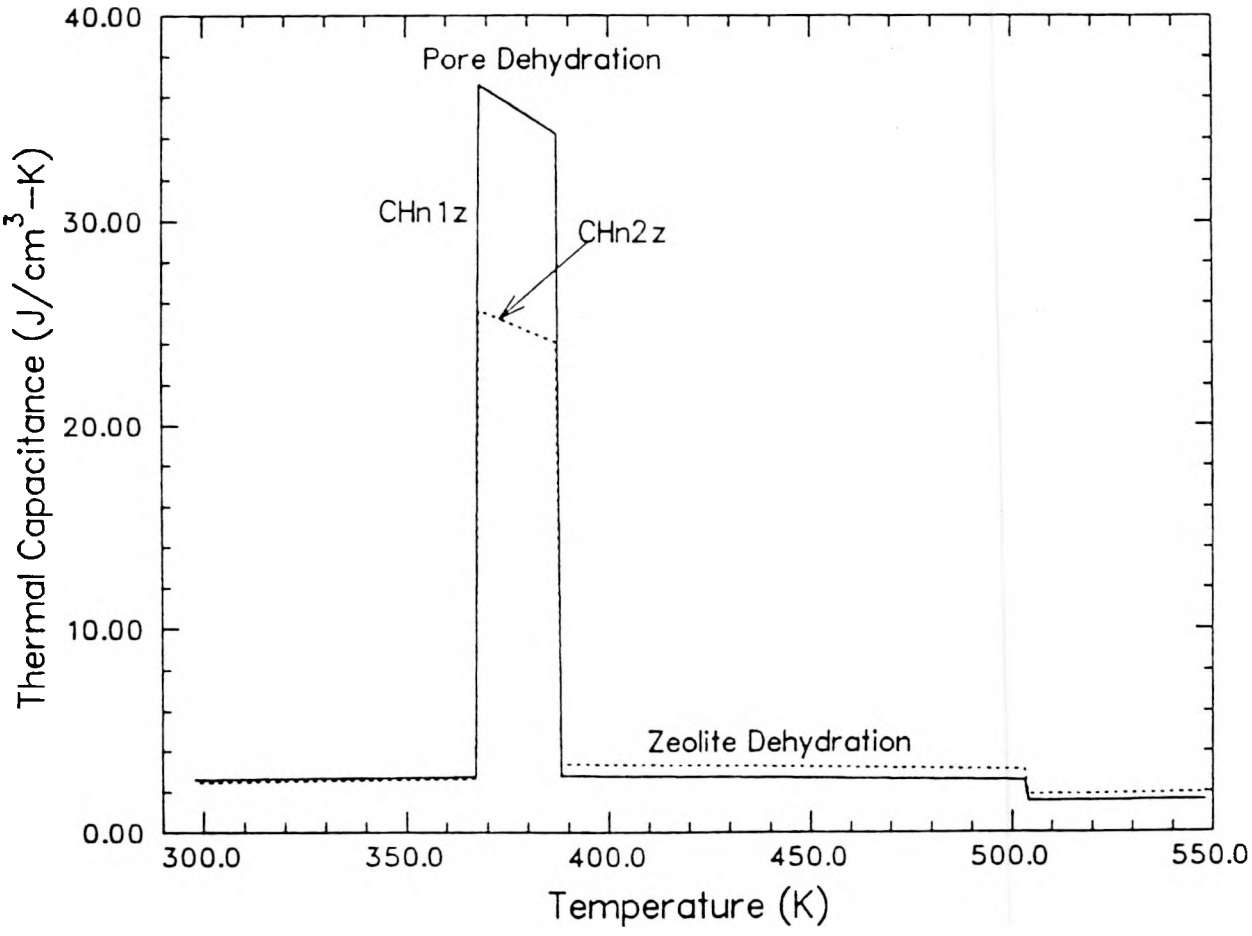

Figure 14. Rock-Mass Thermal Capacitances of Zeolitized Units

4.0 DISCUSSION OF ASSUMPTIONS

The calculations described in this report have required that a large number of assumptions be made. In the following sections, many of the assumptions are discussed; each discussion includes (1) an assessment of the impact on the estimated thermal capacitances if the assumption is wrong, and (2) a brief consideration of how the validity of the assumption might best be tested.

4.1 Calculation of Heat Capacities

The primary assumption used for this report is that accurate values of the heat capacities of solid material can be calculated from bulk chemical composition. If this assumption is wrong, all values calculated using the equations in Appendix A would be incorrect. The magnitude of discrepancies between calculated values and values determined by direct measurement is not expected to be large, because Kopp's rule has been used successfully for many years. Experimental data to be obtained in the near future on tuff samples will allow a rigorous test of the assumption.

4.2 Adequacy of Sampling

The calculations in this report use chemical compositions for 20 samples of the tuffs at Yucca Mountain. Implicit in the calculations is the assumption that these samples adequately represent the natural variation in the composition of the tuffs. Examination of Figures 7, 9, and 10 suggests that other samples would need to have drastically different compositions to cause a significant difference in the calculated heat capacities for the solid components.

Bulk chemical analyses in Scott and Castellanos (1984) and Broxton et al. (1986) as well as unpublished SNL data were compared with the average analyses in Tables 3, 4, and 5. All samples of devitrified and vitric material that were not contaminated by weathering deposits had oxide abundances within 3σ of the mean values in Table 3 and 4, and only 3% of the oxide amounts were more than 2σ from the relevant mean value.

The compositions of zeolitized material were more variable, but eight of nine samples had oxide abundances within 3σ of the mean values in Table 5 (approximately 10% of data between 2σ and 3σ). The single exception is a sample from the lower part of Unit CHnlz in USW G-2, for which the H_2O^+ content was measured as 2.44 wt%. This H_2O^+ abundance is even lower than the mean value for vitric material (Table 4), suggesting that the sample may have undergone significant drying before the chemical analysis was performed.

The preliminary conclusion can be drawn that the 20 samples discussed in this report provide an adequate sampling of the three major lithologies at Yucca Mountain. This conclusion should be reexamined when additional bulk chemistry data become available.

4.3 Data for Oxides

4.3.1 Temperature Dependence

Heat capacity data for oxides have been the object of experiments for many years, and the experimental values are considered to be accurate with an insignificant amount of uncertainty. Representation of the data as a function of temperature is the subject of continuing debate as to which powers of temperature should be included in a fit to experimental data. Several types of equations have been proposed other than the one selected for this report (Equation 1). However, all of the equations are used to obtain statistically optimized fits to experiment data. Thus, the specific choice should not have a significant effect on calculated values of heat capacity.

4.3.2 Choice of Data for SiO_2

For crystalline samples, heat capacity data for quartz were used in this report to calculate the contribution of SiO_2 to the total heat capacity. In the tuffs, SiO_2 is present in several forms; devitrified tuffs contain tridymite, cristobalite, and quartz, and zeolitized tuffs contain quartz and opal-CT. Comparison of data for the heat capacities of

quartz, tridymite, and cristobalite as given by Thompson and Wenemer (1979) and Richet et al. (1982) indicate that differences are less than 1% at temperatures outside the intervals of phase transformations. Thus, use of quartz data for the heat capacity of all SiO_2 in devitrified samples should have little or no effect on the calculations.

Opal-CT is a hydrated form of SiO_2 with intermixed layers of cristobalite and tridymite. Except for the water content, the heat capacity should be similar to the three anhydrous polymorphs of SiO_2 discussed above. For zeolitized tuffs, the water (H_2O^+) has been treated as if it were all present in zeolites as either hydrate or hydroxyl water. Water in opal-CT probably can be treated as hydrate water, so the contribution to total heat capacity already has been included. Thus, use of data for quartz for the heat capacity of SiO_2 in zeolitized samples should not introduce significant errors.

4.3.3 Types of Water in Minerals

The different choices available for the types of water in the minerals and the heat capacity function for each type are discussed in Section 2.4.2. If the assignments of H_2O^+ to the different water types are incorrect, significant errors in the calculated heat capacities of the solid components may be present. The accuracy of the calculated heat capacities can be tested by performing direct measurements of the heat capacities of samples from each lithology.

4.4 Water in Zeolitized and Vitric Samples

In obtaining the chemical compositions to use for calculation of heat capacities, the assumption was made that all H_2O^- was adsorbed water. This assumption is almost certainly correct for devitrified tuffs. However, some fraction of the water measured as H_2O^- for vitric and zeolitized tuffs actually may be an integral part of the phases in the rock and should be treated as H_2O^+. Because water makes a large contribution to the heat capacity of the solid material, errors in the amount of H_2O^+ may affect the calculated heat capacities significantly. The degree to which the H_2O^+

content may have been underestimated in zeolitized and vitric samples will be evaluated during development of procedures for heat capacity measurement.

4.5 SiO_2 Transformations

4.5.1 Temperature Ranges

The transformations of cristobalite and tridymite were assumed to occur over 20°C ranges in temperature for this study. This assumption will almost certainly be incorrect for specific samples, because the transformation intervals can vary with microstructure, crystalline solution, and grain size (Sosman, 1965). However, the total heat absorbed during a transformation should be accurately represented, so the only significant uncertainties associated with the assumption are the accuracy of the assumed onset of each transition and the exact amount of heat absorbed for each degree rise in temperature during the transition. Experimental heat capacities will provide insight on the validity of the assumption.

4.5.2 Amounts of SiO_2 Phases

Mean values were used to represent the abundances of cristobalite and tridymite in the devitrified tuffs. Clearly, the magnitudes of the heat capacities of devitrified tuffs will be sample-specific at temperatures within the transformation intervals. In these intervals, individual heat capacities may differ from heat capacities calculated using mean values by a factor of two because of variations in the abundances of tridymite and cristobalite. Exact heat capacity values to be used in calculations of the thermal response of devitrified tuff during a heater test or in the immediate vicinity of a waste canister will need to be calculated using mineralogic data from site-specific samples.

4.6 Linearization

A number of temperature-dependent properties and processes (other than the heat capacity of oxides) have been used in the calculations in this

report. In each case, the temperature dependence has been assumed to be linear. For the properties of water, the assumption of linearity should not introduce significant error because interpolation intervals between experimental data are relatively small. For the other processes (dehydration of zeolites, dehydration of pores, SiO_2 transformations), it is probable that the temperature dependence is not linear. However, the total amount of heat absorbed during each process should be accurately represented. The only uncertainties introduced by the assumptions are in the distribution of heat capacity and in the exact temperature intervals in which the processes occur. These uncertainties will be evaluated during direct measurements of heat capacity.

4.7 Glass Dehydration

The calculations of heat capacity for vitric units assume that all H_2O^+ remains in the glass during heating. This assumption is unlikely to be valid; therefore the estimates of heat capacities above 100°C probably are somewhat high. Determination of the magnitude of the error will be made during direct measurements of heat capacity.

4.8 Zeolite Dehydration

The assumed linear temperature dependence of zeolite dehydration is discussed in Section 4.6. There are two other potential errors associated with the modeling of the dehydration process. First, the data from Knowlton et al. (1981) for the fractions of water types in zeolites have been assumed to be valid for all zeolites in tuffs at Yucca Mountain. Second, all H_2O^+ in zeolitized samples has been assumed to be contained entirely in zeolites, whereas clay and opal-CT also are usually present in these samples, and perlitic glass is present in some samples. Bish and Chipera (1986) report up to 35 wt% opal-CT and up to 4 wt% clay in zeolitized tuffs. However, the water contents of these phases, especially opal-CT, has not been quantified. Thus, the validity of the two assumptions cannot be evaluated until direct heat capacity measurements are made.

4.9 In Situ Saturation

The values of in situ saturation used in Equation 10 have been taken from Montazer and Wilson (1984). The accuracy of these values has not been verified. Any significant changes to the values would result in significant changes in calculated thermal capacitances.

4.10 Boiling of Pore Water

4.10.1 Temperature Range

The assumed linear temperature dependence of pore-water boiling is discussed in Section 4.6. The range of temperature (20°C) over which boiling is assumed to occur is arbitrary; the very existence of a temperature range for boiling is predicated on laboratory observations of drying rates. Because the temperature range is expected to be dependent on the heating rate, different portions of the rock surrounding a repository would experience temperature ranges of different magnitudes. Observation of thermohydrologic phenomena caused by in situ heater tests should allow at least a partial evaluation of the validity of using a 20°C-range to represent average behavior for pore-water boiling.

4.10.2 Pore-Pressure Effects

The hydrologic properties of the tuffs can affect pore-water boiling in two ways. First, the low permeabilities of the tuffs can inhibit water (and gas) movement and cause local elevations of pore pressures during heating. In turn, higher pore pressures would cause boiling to be delayed to higher temperatures. This effect probably is the primary reason for the temperature range for boiling of pore water in laboratory samples.

The second effect is speculative at this point. In tuffs in the unsaturated zone, pore pressures are negative because of capillary forces. Thus, the normal relationship between atmospheric pressure and boiling temperature may be perturbed in situ. The effect is probably small, as has

been assumed implicitly in calculating the lower boiling temperature (Section 3.4). This effect and the effect discussed in the preceding paragraph also will need to be evaluated during in situ heater tests.

4.11 Mineralogy of Unit PTn

Unit PTn has been assumed to be vitric for the calculations in this report. Mineralogic data in Bish and Vaniman (1985) and Bish and Chipera (1986) indicate that, even for core holes in which welded, devitrified ash flows are absent, samples of Unit PTn are a mixture of glass, clay, and devitrification products. Two adjustments should be made to improve the modeling of Unit PTn. First, the SiO_2 content should be distributed between quartz and silica glass. Second, H_2O^+ should be divided into hydroxyl water (in clay) and perlitic water (in glass). The net effect of these changes would probably be to decrease the heat capacity of the solid component because of the relatively large difference in the heat capacities of the two water types. The magnitude of the change would need to be evaluated on a sample-specific basis, because the mineralogy of individual samples would be a major factor.

5.0 CONCLUSIONS

The major result of this study is the compilation of preliminary thermal capacitance data provided in Table 9, Figures 12 through 14, and Appendix A. Subsidiary results are the estimates of average heat capacities for the solid components of devitrified, vitric, and zeolitized samples. These heat capacities should be validated by experimentally determined data as soon as practicable. This is particularly important because many of the assumptions discussed in Section 4 cannot be evaluated at present.

One substantial caveat must be stated as part of these conclusions. For temperatures ≥95°C, the thermal capacitances given here apply only during heating of the tuffs. Too little is known about the rehydration of the tuffs and hydrous phases therein to adequately model thermal capacitances as a function of temperature during cooling. Exact reproducibility of the curves shown in Figures 12 through 14 can be assumed as a first estimate if cooling behavior is to be calculated, but the user is forewarned that cooling may well occur faster than rehydration. If so, the thermal capacitances given here will overestimate the "real" in situ values.

6.0 REFERENCES

Bish, D. L., and S. J. Chipera, 1986. Mineralogy of Drill Holes J-13, UE-25A#1, and USW G-1 at Yucca Mountain, Nevada; LA-10764-MS, Los Alamos National Laboratory, Los Alamos, NM. (HQS.880517.1957)

Bish, D. L., and D. T. Vaniman, 1985. Mineralogic Summary of Yucca Mountain, Nevada; LA-10543-MS, Los Alamos National Laboratory, Los Alamos, NM. (NNA.870407.0330)

Brandshaug, T., 1991. A Sensitivity Study of the Thermomechanical Far-Field Model of Yucca Mountain; SAND87-7079, Sandia National Laboratories, Albuquerque, NM. (NNA.900111.0001)

Broxton, D. E., R. G. Warren, R. C. Hagan, and G. Luedemann, 1986. Chemistry of Diagenetically Altered Tuffs at a Potential Nuclear Waste Repository, Yucca Mountain, Nye County, Nevada; LA-10802-MS, Los Alamos National Laboratory, Los Alamos, NM. (NNA.890327.0036)

Connolly, J. R., and F. B. Nimick, 1990. Mineralogic and Chemical Data Supporting Heat Capacity Determination for Tuffaceous Rocks; SAND88-0882, Sandia National Laboratories, Albuquerque, NM. (NNA.890928.0125)

DOE (U.S. Department of Energy, Nevada Operations Office), 1987. Exploratory Shaft Facility Subsystem Design Requirements Document; NVO-309, U.S. Dept. of Energy, Nevada Operations Office, Las Vegas, NV. (NNA.871228.0041)

Haas, J. L., Jr., 1974. PHAS20, A Program for Simultaneous Multiple Regression of a Mathematical Model to Thermochemical Data; U. S. Department of Commerce, National Technical Information Service, AD-780 301. (NNA.900515.0008)

Haas, J. L., Jr., and J. R. Fisher, 1976. Simultaneous Evaluation and Correlation of Thermodynamic Data; American Journal of Science, v. 276, pp. 525-545. (NNA.900827.0192)

Helgeson, H. C., J. M. Delany, H. W. Nesbitt, and D. K. Bird, 1978. Summary and Critique of the Thermodynamic Properties of the Rock-Forming Minerals; Amer. Jour. Sci., v. 278-A, 229 p. (HQS.880517.2457)

King, E. G., 1955. Low-temperature Heat Capacity and Entropy at 298.15 deg K of Analcite; Journal of the American Chemical Society, v. 87, pp. 2192-2193. (NNA.900917.0123)

King, E. G., S. S. Todd, and K. K. Kelley, 1948. Perlite: Thermal Data and Energy Required for Expansion; USBM-RI-4394, U.S. Bureau of Mines, Pittsburgh, PA. (NNA.900418.0002)

King, E. G. and W. W. Weller, 1961. Low-temperature Heat Capacities and Entropies at 298.15 deg K of Some Sodium- and Calcium-Aluminum Silicates; USBM-RI-5810, U. S. Bureau of Mines, Pittsburgh, PA. (NNA.900418.0003)

REFERENCES
(Continued)

Klavetter, E. A., and R. R. Peters, 1986. Estimation of Hydrologic Properties of an Unsaturated, Fractured Rock Mass; SAND84-2642, Sandia National Laboratories, Albuquerque, NM. (NNA.870317.0738)

Knowlton, G. D., and H. L. McKague, 1976. A Study of the Water Content in Zeolitic Tuffs from the Nevada Test Site; Lawrence Livermore Laboratory Conference Report CONF-760626-1 (UCRL-78013), 15 p. plus figures. (NNA.890515.0130)

Knowlton, G. D., T. R. White, and H. L. McKague, 1981. Thermal Study of Types of Water Associated with Clinoptilolite; Clays and Clay Minerals, v. 29, no. 5, pp. 403-411. (NNA.900419.0003)

Kopp, H., 1864. Ueber die specifische warme der starren korper; Annalen der Chemie und Pharmacie, Supplementband, v. 3, pp. 289-342. (NNA.900515.0009)

Montazer, P., and W. E. Wilson, 1984. Conceptual Hydrologic Model of Flow in the Unsaturated Zone, Yucca Mountain, Nevada; USGS-WRIR-84-4345, U. S. Geologic Survey, Denver, CO. (HQS.880517.1675)

Nash, L. K, 1971. CHEMTHERMO: A Statistical Approach to Classical Chemical Thermodynamics; Addison-Wesley Publishing Company (Reading, MA), p. 74. (NNA.900404.0133)

Nimick, F. B., 1990. The Thermal Conductivity of the Topopah Spring Member at Yucca Mountain, Nevada; SAND86-0090, Sandia National Laboratories, Albuquerque, NM. (NNA.890516.0183)

Nimick, F. B., and B. M. Schwartz, 1987. Bulk, Thermal, and Mechanical Properties of the Topopah Spring Member of the Paintbrush Tuff, Yucca Mountain, Nevada; SAND85-0762, Sandia National Laboratories, Albuquerque, NM. (NNA.871013.0012)

Nimick, F. B., L. E. Shephard, and T. E., Blejwas, 1988. Preliminary Evaluation of the Exploratory Shaft Representativeness for the Yucca Mountain Project; SAND87-1685, Sandia National Laboratories, Albuquerque, NM. (NNA.900510.0022)

Ortiz, T. S., R. L. Williams, F. B. Nimick, B. C. Whittet, and D. L. South, 1985. A Three-Dimensional Model of Reference Thermal/Mechanical and Hydrological Stratigraphy at Yucca Mountain, Southern Nevada; SAND84-1076, Sandia National Laboratories, Albuquerque, NM. (NNA.890315.0013)

Pankratz, L. B., 1964. High-temperature Heat Contents and Entropies of Muscovite and Dehydrated Muscovite; USBM-RI-6371, U.S. Bureau of Mines, Pittsburgh, PA. (NNA.900418.0004)

Pankratz, L. B., 1968. High-temperature Heat Contents and Entropies of Dehydrated Analcite, Kaliophilite, and Leucite; USBM-RI-7073, U.S. Bureau of Mines, Pittsburgh, PA. (NNA.900515.0010)

REFERENCES
(Concluded)

Richet, P., Y. Bottinga, L. Denielou, J. P. Petitet, and C. Tequi, 1982. Thermodynamic Properties of Quartz, Cristobalite, and Amorphous SiO_2: Drop Calorimetry Measurements Between 1000 and 1800 K and a Review from 0 to 2000 K; Geochim. Cosmochim. Acta, v. 46, pp. 2639-2658. (NNA.900419.0004)

Robie, R. A., B. S. Hemingway, and J. R. Fisher, 1978. Thermodynamic Properties of Minerals and Related Substances at 298.15 K and 1 bar (105 Pascals) Pressure and at Higher Temperatures; U. S. Geological Survey Bulletin 1452, 456 p. (NNA.900702.0002)

Robinson, G. R., and J. L. Haas, Jr., 1983. Heat Capacity, Relative Enthalpy and Calorimetric Entropy of Silicate Minerals: An Empirical Method of Prediction; Amer. Min., v. 68, pp. 551-553. (NNA.900417.0030)

Scott, R. B., and M. Castellanos, 1984. Stratigraphic and Structural Relations of Volcanic Rocks in Drill Holes USW GU-3 and USW G-3, Yucca Mountain, Nye County, Nevada; USGS-OFR-84-491, U.S. Geological Survey, Denver, CO. (NNA.890804.0017)

Scott, R. B., R. W. Spengler, S. Diehl, A. R. Lappin, and M. P. Chornack, 1983. Geologic Character of Tuffs in the Unsaturated Zone at Yucca Mountain, Southern Nevada; in J. Mercer (ed.), Role of the Unsaturated Zone in Radioactive and Hazardous Waste Disposal; Ann Arbor Science Publishers (Ann Arbor, MI), pp. 289-335. (NNA.870406.0034)

Shahid, K. A., and F. P. Glasser, 1970. Thermal Properties of Tyridymite: 25°C - 300°C; J. Therm. Analysis, v. 2, pp. 181-190. (NNA.900419.0005)

Sosman, R. B., 1965. The Phases of Silica; Rutgers University Press (New Brunswick, NJ), pp. 102-103, 112-115. (NNA.900720.0070)

Spengler, R. W. and M. P. Chornack, 1984. Stratigraphic and Structural Characteristics of Volcanic Rocks in Core Hole USW G-4, Yucca Mountain, Nye County, Nevada, with a section on geophysical logs by D. C. Muller and J. Kibler; USGS-OFR-84-789, U. S. Geological Survey, Denver, CO. (NNA.870519.0105)

Thompson, A. B., and M. Wennemer, 1979. Heat Capacities and Inversions in Tridymite, Cristobalite, and Tridymite-Cristobalite Mixed Phases; Amer. Min., v. 64, pp. 1018-1026. (NNA.900419.0006)

Tillerson, J. R., and F. B. Nimick (eds.), 1984. Geoengineering Properties of Potential Repository Units at Yucca Mountain, Southern Nevada; SAND84-0221, Sandia National Laboratories, Albuquerque, NM. (NNA.870406.0308)

APPENDIX A

EQUATIONS FOR CALCULATION OF THERMAL CAPACITANCE

The following pages list the equations used to calculate the thermal capacitance of each of nine thermal/mechanical units as a function of temperature. The curves obtained using these equations are plotted in Figures 12, 13, and 14 in Section 3.5.

UNIT TCw

25°-94°C: $1.8306 + 7.4523\times10^{-4}T + 1.1898\times10^{-2}T^{1/2} + 8.3361\times10^{-8}T^{2} - 4.2481T^{-1/2} + 3.8259\times10^{-4}T^{-1} - 3.3656\times10^{+4}T^{-2} + 0.07169\rho_{w}C_{p,w}$

95°-114°C: $1.8306 + 7.4523\times10^{-4}T + 1.1898\times10^{-2}T^{1/2} + 8.3361\times10^{-8}T^{2} - 4.2481T^{-1/2} + 3.8259\times10^{-4}T^{-1} - 3.3656\times10^{+4}T^{-2} + 0.07169\rho_{w}C_{p,w}(20.3763 - 0.0526T) + 3.5845\times10^{-3}\rho_{w}\Delta H_{boil}$

115°-152°C: $1.8306 + 7.4523\times10^{-4}T + 1.1898\times10^{-2}T^{1/2} + 8.3361\times10^{-8}T^{2} - 4.2481T^{-1/2} + 3.8259\times10^{-4}\ T^{-1} - 3.3656\times10^{+4}T^{-2}$

153°-172°C: $1.8306 + 7.4523\times10^{-4}T + 1.1898\times10^{-2}T^{1/2} + 8.3361\times10^{-8}T^{2} - 4.2481T^{-1/2} + 3.8259\times10^{-4}\ T^{-1} - 3.3656\times10^{+4}T^{-2} + 0.0049$

173°-214°C: $1.8306 + 7.4523\times10^{-4}T + 1.1898\times10^{-2}T^{1/2} + 8.3361\times10^{-8}T^{2} - 4.2481T^{-1/2} + 3.8259\times10^{-4}\ T^{-1} - 3.3656\times10^{+4}T^{-2}$

215°-234°C: $1.8306 + 7.4523\times10^{-4}T + 1.1898\times10^{-2}T^{1/2} + 8.3361\times10^{-8}T^{2} - 4.2481T^{-1/2} + 3.8259\times10^{-4}\ T^{-1} - 3.3656\times10^{+4}T^{-2} + 0.5432$

235°-275°C: $1.8306 + 7.4523\times10^{-4}T + 1.1898\times10^{-2}T^{1/2} + 8.3361\times10^{-8}T^{2} - 4.2481T^{-1/2} + 3.8259\times10^{-4}\ T^{-1} - 3.3656\times10^{+4}T^{-2}$

UNIT PTn

25°-94°C: $1.6281 + 2.6079\times10^{-4}T + 4.8068\times10^{-3}T^{1/2} + 1.2831\times10^{-7}T^{2} - 1.8330T^{-1/2} + 1.5456\times10^{-4}T^{-1} - 5.7369\times10^{+4}T^{-2} + 0.3538\rho_{w}C_{p,w}$

95°-114°C: $1.6281 + 2.6079\times10^{-4}T + 4.8068\times10^{-3}T^{1/2} + 1.2831\times10^{-7}T^{2} - 1.8330T^{-1/2} + 1.5456\times10^{-4}T^{-1} - 5.7369\times10^{+4}T^{-2} + 0.3538\rho_{w}C_{p,w}(20.3763 - 0.0526T) + 1.281\times10^{-2}\rho_{w}\Delta H_{boil}$

115°-275°C: $1.6281 + 2.6079\times10^{-4}T + 4.8068\times10^{-3}T^{1/2} + 1.2831\times10^{-7}T^{2} - 1.8330T^{-1/2} + 1.5456\times10^{-4}T^{-1} - 5.7369\times10^{+4}T^{-2}$

UNIT TSw1

25°-94°C: $1.7620 + 7.1731\times10^{-4}T + 1.1452\times10^{-2}T^{1/2} + 8.0237\times10^{-8}T^{2} - 4.0889T^{-1/2} + 3.6826\times10^{-4}T^{-1} - 3.2395\times10^{+4}T^{-2} + 9.5596\times10^{-2}\rho_{w}C_{p,w}$

95°-114°C: $1.7620 + 7.1731\times10^{-4}T + 1.1452\times10^{-2}T^{1/2} + 8.0237\times10^{-8}T^{2} - 4.0889T^{-1/2} + 3.6826\times10^{-4}T^{-1} - 3.2395\times10^{+4}T^{-2} + 9.5596\times10^{-2}\rho_{w}C_{p,w}(20.3763 - 0.0526T) + 4.7798\times10^{-3}\rho_{w}\Delta H_{boil}$

115°-152°C: $1.7620 + 7.1731\times10^{-4}T + 1.1452\times10^{-2}T^{1/2} + 8.0237\times10^{-8}T^{2} - 4.0889T^{-1/2} + 3.6826\times10^{-4}T^{-1} - 3.2395\times10^{+4}T^{-2}$

153°-172°C: $1.7620 + 7.1731\times10^{-4}T + 1.1452\times10^{-2}T^{1/2} + 8.0237\times10^{-8}T^{2} - 4.0889T^{-1/2} + 3.6826\times10^{-4}T^{-1} - 3.2395\times10^{+4}T^{-2} + 0.0177$

173°-214°C: $1.7620 + 7.1731\times10^{-4}T + 1.1452\times10^{-2}T^{1/2} + 8.0237\times10^{-8}T^{2} - 4.0889T^{-1/2} + 3.6826\times10^{-4}T^{-1} - 3.2395\times10^{+4}T^{-2}$

215°-234°C: $1.7620 + 7.1731\times10^{-4}T + 1.1452\times10^{-2}T^{1/2} + 8.0237\times10^{-8}T^{2} - 4.0889T^{-1/2} + 3.6826\times10^{-4}T^{-1} - 3.2395\times10^{+4}T^{-2} + 0.2993$

235°-275°C: $1.7620 + 7.1731\times10^{-4}T + 1.1452\times10^{-2}T^{1/2} + 8.0237\times10^{-8}T^{2} - 4.0889T^{-1/2} + 3.6826\times10^{-4}T^{-1} - 3.2395\times10^{+4}T^{-2}$

UNIT TSw2

25°-94°C: $1.9053 + 7.7564\times10^{-4}T + 1.2384\times10^{-2}T^{1/2} + 8.6762\times10^{-8}T^{2} - 4.4214T^{-1/2} + 3.9821\times10^{-4}T^{-1} - 3.5030\times10^{+4}T^{-2} + 7.7864\times10^{-2}\rho_{w}C_{p,w}$

95°-114°C: $1.9053 + 7.7564\times10^{-4}T + 1.2384\times10^{-2}T^{1/2} + 8.6762\times10^{-8}T^{2} - 4.4214T^{-1/2} + 3.9821\times10^{-4}T^{-1} - 3.5030\times10^{+4}T^{-2} + 7.7864\times10^{-2}\rho_{w}C_{p,w}(20.3763 - 0.0526T) + 3.8932\times10^{-3}\rho_{w}\Delta H_{boil}$

115°-152°C: $1.9053 + 7.7564\times10^{-4}T + 1.2384\times10^{-2}T^{1/2} + 8.6762\times10^{-8}T^{2} - 4.4214T^{-1/2} + 3.9821\times10^{-4}T^{-1} - 3.5030\times10^{+4}T^{-2}$

153°-172°C: $1.9053 + 7.7564\times10^{-4}T + 1.2384\times10^{-2}T^{1/2} + 8.6762\times10^{-8}T^{2} - 4.4214T^{-1/2} + 3.9821\times10^{-4}T^{-1} - 3.5030\times10^{+4}T^{-2} + 0.0066$

173°-214°C: $1.9053 + 7.7564\times10^{-4}T + 1.2384\times10^{-2}T^{1/2} + 8.6762\times10^{-8}T^{2} - 4.4214T^{-1/2} + 3.9821\times10^{-4}T^{-1} - 3.5030\times10^{+4}T^{-2}$

215°-234°C: $1.9053 + 7.7564\times10^{-4}T + 1.2384\times10^{-2}T^{1/2} + 8.6762\times10^{-8}T^{2} - 4.4214T^{-1/2} + 3.9821\times10^{-4}T^{-1} - 3.5030\times10^{+4}T^{-2} + 0.3539$

235°-275°C: $1.9053 + 7.7564\times10^{-4}T + 1.2384\times10^{-2}T^{1/2} + 8.6762\times10^{-8}T^{2} - 4.4214T^{-1/2} + 3.9821\times10^{-4}T^{-1} - 3.5030\times10^{+4}T^{-2}$

UNIT TSw3

25°-94°C: $2.7286 + 4.3706\times10^{-4}T + 8.0559\times10^{-3}T^{1/2} + 2.1505\times10^{-7}T^{2} - 3.0720T^{-1/2} + 2.5904\times10^{-4}T^{-1} - 9.6148\times10^{+4}T^{-2} + 2.08\times10^{-2}\rho_{w}C_{p,w}$

95°-114°C: $2.7286 + 4.3706\times10^{-4}T + 8.0559\times10^{-3}T^{1/2} + 2.1505\times10^{-7}T^{2} - 3.0720T^{-1/2} + 2.5904\times10^{-4}T^{-1} - 9.6148\times10^{+4}T^{-2} + 2.08\times10^{-2}\rho_{w}C_{p,w}(20.3763 - 0.0526T) + 1.04\times10^{-3}\rho_{w}\Delta H_{boil}$

115°-275°C: $2.7286 + 4.3706\times10^{-4}T + 8.0559\times10^{-3}T^{1/2} + 2.1505\times10^{-7}T^{2} - 3.0720T^{-1/2} + 2.5904\times10^{-4}T^{-1} - 9.6148\times10^{+4}T^{-2}$

UNIT CHn1v

25°-94°C: $1.7848 + 2.8588\times10^{-4}T + 5.2694\times10^{-3}T^{1/2} + 1.4066\times10^{-7}T^{2} - 2.0094T^{-1/2} + 1.6944\times10^{-4}T^{-1} - 6.2890\times10^{+4}T^{-2} + 0.3105\rho_{w}C_{p,w}$

95°-114°C: $1.7848 + 2.8588\times10^{-4}T + 5.2694\times10^{-3}T^{1/2} + 1.4066\times10^{-7}T^{2} - 2.0094T^{-1/2} + 1.6944\times10^{-4}T^{-1} - 6.2890\times10^{+4}T^{-2} + 0.3105\rho_{w}C_{p,w}(20.3763 - 0.0526T) + 1.5525\times10^{-2}\rho_{w}\Delta H_{boil}$

115°-275°C: $1.7848 + 2.8588\times10^{-4}T + 5.2694\times10^{-3}T^{1/2} + 1.4066\times10^{-7}T^{2} - 2.0094T^{-1/2} + 1.6944\times10^{-4}T^{-1} - 6.2890\times10^{+4}T^{-2}$

UNIT CHn2v

<u>25°-94°C:</u> $2.0943 + 3.3546\times10^{-4}T + 6.1831\times10^{-3}T^{1/2} + 1.6505\times10^{-7}T^{2} - 2.3578T^{-1/2} + 1.9882\times10^{-4}T^{-1} - 7.3796\times10^{+4}T^{-2} + 0.2529\rho_{w}C_{p,w}$

<u>95°-114°C:</u> $2.0943 + 3.3546\times10^{-4}T + 6.1831\times10^{-3}T^{1/2} + 1.6505\times10^{-7}T^{2} - 2.3578T^{-1/2} + 1.9882\times10^{-4}T^{-1} - 7.3796\times10^{+4}T^{-2} + 0.2529\rho_{w}C_{p,w}(20.3763 - 0.0526T) + 1.2645\times10^{-2}\rho_{w}\Delta H_{boil}$

<u>115°-275°C:</u> $2.0943 + 3.3546\times10^{-4}T + 6.1831\times10^{-3}T^{1/2} + 1.6505\times10^{-7}T^{2} - 2.3578T^{-1/2} + 1.9882\times10^{-4}T^{-1} - 7.3796\times10^{+4}T^{-2}$

UNIT CHn1z

25°-94°C: $1.6440 + 4.2844\times10^{-4}T + 1.0999\times10^{-2}T^{1/2} + 7.7058\times10^{-8}T^{2} - 6.0844T^{-1/2} + 3.5366\times10^{-4}T^{-1} - 2.2823\times10^{+4}T^{-2} + 0.2985\rho_{w}C_{p,w}$

95°-114°C: $1.6440 - 0.2390(-2.7270 + 7.4074\times10^{-3}T) + 4.2844\times10^{-4}T + 1.0999\times10^{-2}T^{1/2} + 7.7058\times10^{-8}T^{2} + (-6.0844 + 1.1079(-2.7270 + 7.4074\times10^{-3}T))T^{-1/2} + 3.5366\times10^{-4}T^{-1} - 2.2823\times10^{+4}T^{-2} + 0.2985\rho_{w}C_{p,w}(20.3763 - 0.0526T) + (1.4924\times10^{-2}\rho_{w} + 0.00056)\ \Delta H_{boil}$

115°-230°C: $1.6440 - 0.2390(-2.7270 + 7.4074\times10^{-3}T) + 4.2844\times10^{-4}T + 1.0999\times10^{-2}T^{1/2} + 7.7058\times10^{-8}T^{2} + (-6.0844 + 1.1079(-2.7270 + 7.4074\times10^{-3}T))T^{-1/2} + 3.5366\times10^{-4}T^{-1} - 2.2823\times10^{+4}T^{-2} + 0.00056\Delta H_{boil}$

231°-275°C: $1.4050 + 4.2844\times10^{-4}T + 1.0999\times10^{-2}T^{1/2} + 7.7058\times10^{-8}T^{2} - 4.9764\ T^{-1/2} + 3.5366\times10^{-4}T^{-1} - 2.2823\times10^{+4}T^{-2}$

UNIT CHn2z

25°-94°C: $1.9830 + 5.1679\times10^{-4}T + 1.3267\times10^{-2}T^{1/2} + 9.2949\times10^{-8}T^{2} - 7.3391T^{-1/2} + 4.2659\times10^{-4}T^{-1} - 2.7529\times10^{+4}T^{-2} + 0.1966\rho_{w}C_{p,w}$

95°-114°C: $1.9830 - 0.2883(-2.7270 + 7.4074\times10^{-3}T) + 5.1679\times10^{-4}T + 1.3267\times10^{-2}T^{1/2} + 9.2949\times10^{-8}T^{2} + (-7.3391 + 1.3364(-2.7270 + 7.4074\times10^{-3}T))T^{-1/2} + 4.2659\times10^{-4}T^{-1} - 2.7529\times10^{+4}T^{-2} + 0.1966\rho_{w}C_{p,w}(20.3763 - 0.0526T) + (6.755\times10^{-4} + 9.828\times10^{-3}\rho_{w})\Delta H_{boil}$

115°-230°C: $1.9830 - 0.2883(-2.7270 + 7.4074\times10^{-3}T) + 5.1679\times10^{-4}T + 1.3267\times10^{-2}T^{1/2} + 9.2949\times10^{-8}T^{2} + (-7.3391 + 1.3364(-2.7270 + 7.4074\times10^{-3}T))T^{-1/2} + 4.2659\times10^{-4}T^{-1} - 2.7529\times10^{+4}T^{-2} + 6.755 \times 10^{-4}\Delta H_{boil}$

231°-275°C: $1.6391 + 5.1679\times10^{-4}T + 1.3267\times10^{-2}T^{1/2} + 9.2949\times10^{-8}T^{2} - 6.0027T^{-1/2} + 4.2659\times10^{-4}T^{-1} - 2.7529\times10^{+4}T^{-2}$

APPENDIX B

INFORMATION FROM, AND CANDIDATE INFORMATION FOR, THE SITE AND ENGINEERING PROPERTY DATA BASE AND THE REFERENCE INFORMATION BASE

No information in this report has been taken from, nor is intended for entry into, the Site and Engineering Property Data Base (SEPDB). However, the chemical analyses in Table 1 were submitted to the SEPDB as candidate data early in 1989.

The information presented in Equations 3, 6 and 7, Table 9, Figures 12 through 14, and Appendix A is candidate information for the reference information base (RIB). Information taken from the RIB (Version 4) consists of in situ saturation values (Revision 0 of Section 1.4.2), grain densities and matrix porosities (Revision 0 of Section 1.2.1), and data for the thermal/mechanical stratigraphy at USW G-4 (Revision 0 of Section 1.1.2).

DISTRIBUTION LIST

1 John W. Bartlett, Director (RW-1)
Office of Civilian Radioactive
Waste Management
U.S. Department of Energy
Forrestal Bldg.
Washington, D.C. 20585

1 F. G. Peters, Deputy Director (RW-2)
Office of Civilian Radioactive
Waste Management
U.S. Department of Energy
Forrestal Bldg.
Washington, D.C. 20585

1 D. G. Horton (RW-3)
Office of Quality Assurance
Office of Civilian Radioactive
Waste Management
U.S. Department of Energy
Forrestal Bldg.
Washington, D.C. 20585

1 T. H. Isaacs (RW-4)
Office of Strategic Planning
and International Programs
Office of Civilian Radioactive
Waste Management
U.S. Department of Energy
Forrestal Bldg.
Washington, D.C. 20585

1 J. D. Saltzman (RW-5)
Office of External Relations
Office of Civilian Radioactive
Waste Management
U.S. Department of Energy
Forrestal Bldg.
Washington, D.C. 20585

1 Samuel Rousso (RW-10)
Office of Program and Resources
Management
Office of Civilian Radioactive
Waste Management
U.S. Department of Energy
Forrestal Bldg.
Washington, D.C. 20585

1 Carl P. Gertz (RW-20)
Office of Geologic Disposal
Office of Civilian Radioactive
Waste Management
U.S. Department of Energy
Forrestal Bldg.
Washington, D.C. 20585

1 D. E. Shelor (RW-30)
Office of Systems and Compliance
Office of Civilian Radioactive
Waste Management
U.S. Department of Energy
Forrestal Bldg.
Washington, D.C. 20585

1 L. H. Barrett (RW-40)
Office of Storage and Transportation
Office of Civilian Radioactive
Waste Management
U.S. Department of Energy
Forrestal Bldg.
Washington, D.C. 20585

1 F. G. Peters (RW-50)
Office of Contractor Business
Management
Office of Civilian Radioactive
Waste Management
U.S. Department of Energy
Forrestal Bldg.
Washington, D.C. 20585

1 J. C. Bresee (RW-10)
Office of Civilian Radioactive
Waste Management
U.S. Department of Energy
Forrestal Bldg.
Washington, D.C. 20585

1 S. J. Brocoum (RW-20)
Office of Civilian Radioactive
Waste Management
U.S. Department of Energy
Forrestal Building
Washington, D.C. 20585

1 Gerald Parker (RW-30)
Office of Civilian Radioactive
Waste Management
U.S. Department of Energy
Forrestal Bldg.
Washington, D.C. 20585

1 D. U. Deere, Chairman
Nuclear Waste Technical
Review Board
1100 Wilson Blvd. #910
Arlington, VA 22209-2297

5 Carl P. Gertz, Project Manager
Yucca Mountain Project Office
Nevada Operations Office
U.S. Department of Energy
Mail Stop 523
P.O. Box 98518
Las Vegas, NV 89193-8518

1 C. L. West, Director
Office of External Affairs
Nevada Operations Office
U.S. Department of Energy
P.O. Box 98518
Las Vegas, NV 89193-8518

12 Technical Information Office
Nevada Operations Office
U. S. Department of Energy
P.O. Box 98518
Las Vegas, NV 89193-8518

1 P. K. Fitzsimmons, Director
Health Physics & Environmental Division
Nevada Operations Office
U.S. Department of Energy
P.O. Box 98518
Las Vegas, NV 89193-8518

1 Repository Licensing & Quality Assurance Project Directorate
Division of Waste Management
U.S. Nuclear Regulatory Commission
Washington, D.C. 20555

1 Senior Project Manager for Yucca Mountain Repository Project Branch
Division of Waste Management
U.S. Nuclear Regulatory Commission
Washington, D.C. 20555

1 NRC Document Control Desk
Division of Waste Management
U.S. Nuclear Regulatory Commission
Washington, D.C. 20555

1 E. P. Binnall
Field Systems Group Leader
Building 50B/4235
Lawrence Berkeley Laboratory
Berkeley, CA 94720

1 Center for Nuclear Waste Regulatory Analyses
6220 Culebra Road
Drawer 28510
San Antonio, TX 78284

3 L. J. Jardine
Technical Project Officer for YMP
Lawrence Livermore National Laboratory
Mail Stop L-204
P.O. Box 808
Livermore, CA 94550

4 R. J. Herbst
Technical Project Officer for YMP
Los Alamos National Laboratory
N-5, Mail Stop J521
P.O. Box 1663
Los Alamos, NM 87545

1 H. N. Kalia
Exploratory Shaft Test Manager
Los Alamos National Laboratory
Mail Stop 527
101 Convention Center Dr.
Suite 820
Las Vegas, NV 89109

1 J. F. Divine
Assistant Director for Engineering Geology
U.S. Geological Survey
106 National Center
12201 Sunrise Valley Dr.
Reston, VA 22092

6 L. R. Hayes
Technical Project Officer for YMP
U.S. Geological Survey
P.O. Box 25046
421 Federal Center
Denver, CO 80225

1 D. Zesiger
U.S. Geological Survey
101 Convention Center Dr.
Suite 860 - MS509
Las Vegas, NV 89109

1 DeWayne A. Campbell
YMP Technical Project Officer
Bureau of Reclamation
P.O. Box 25007 Bldg. 67
Denver, CO 80225-0007

1 K. W. Causseaux
NHP Reports Chief
U.S. Geological Survey
P.O. Box 25046
421 Federal Center
Denver, CO 80225

1 R. V. Watkins, Chief
Project Planning and Management
U.S. Geological Survey
P.O. Box 25046
421 Federal Center
Denver, CO 80225

1 V. M. Glanzman
U.S. Geological Survey
P.O. Box 25046
913 Federal Center
Denver, CO 80225

1 J. H. Nelson
Technical Project Officer for YMP
Science Applications International Corp.
101 Convention Center Dr.
Suite 407
Las Vegas, NV 89109

2 SAIC-T&MSS Library
Science Applications International Corp.
101 Convention Center Dr.
Suite 407
Las Vegas, NV 89109

1 Elaine Ezra
YMP GIS Project Manager
EG&G Energy Measurements, Inc.
Mail Stop D-12
P.O. Box 1912
Las Vegas, NV 89125

1 W. M. Hewitt, Program Manager
Roy F. Weston, Inc.
955 L'Enfant Plaza, Southwest
Suite 800
Washington, D.C. 20024

1 Technical Information Center
Roy F. Weston, Inc.
955 L'Enfant Plaza, Southwest
Suite 800
Washington, D.C. 20024

1 D. L. Fraser, General Manager
Reynolds Electrical & Engineering Co.
P.O. Box 98521
Mail Stop 555
Las Vegas, NV 89193-8521

1 Robert F. Pritchett
Technical Project Officer for YMP
Reynolds Electrical & Engineering Co.
Mail Stop 615
P.O. Box 98521
Las Vegas, NV 89193-8521

1 A. E. Gurrola
General Manager
Raytheon, Inc.
Mail Stop 580
P.O. Box 93838
Las Vegas, NV 89193-3838

1 James C. Calovini
Raytheon Services, Inc.
101 Convention Center Dr.
Suite P-280
Las Vegas, NV 89109

1 D. L. Lockwood, General Manager
Raytheon Services, Inc.
Mail Stop 514
P.O. Box 93265
Las Vegas, NV 89193-3265

1 Richard L. Bullock
Technical Project Officer for YMP
Raytheon Services, Inc.
101 Convention Center Dr.
Suite P250
Las Vegas, NV 89109

1 R. E. Lowder
Technical Project Officer for YMP
MAC Technical Services
Valley Bank Center
101 Convention Center Drive
Suite 1100
Las Vegas, NV 89109

1 D. J. Bales
Science and Technology Division
Office of Scientific and Technical Information
U.S. Department of Energy
P.O. Box 62
Oak Ridge, TN 37831

1 Carlos G. Bell, Jr.
Professor of Civil Engineering
Civil and Mechanical Engineering Department
University of Nevada, Las Vegas
4505 South Maryland Parkway
Las Vegas, NV 89154

1 C. F. Costa, Director
Nuclear Radiation Assessment Division
U.S. Environmental Protection Agency
Environmental Monitoring Systems Laboratory
P.O. Box 93478
Las Vegas, NV 89193-3478

1 ONWI Library
Battelle Columbus Laboratory
Office of Nuclear Waste Isolation
505 King Avenue
Columbus, OH 43201

1 T. Hay, Executive Assistant
Office of the Governor
State of Nevada
Capitol Complex
Carson City, NV 89710

3 R. R. Loux, Jr.
Executive Director
Nuclear Waste Project Office
State of Nevada
Evergreen Center, Suite 252
1802 North Carson Street
Carson City, NV 89710

1 C. H. Johnson
Technical Program Manager
Nuclear Waste Project Office
State of Nevada
Evergreen Center, Suite 252
1802 North Carson Street
Carson City, NV 89710

1 John Fordham
Water Resources Center
Desert Research Institute
P.O. Box 60220
Reno, NV 89506

1 Dr. Martin Mifflin
Desert Research Institute
Water Resources Center
2505 Chandler Avenue
Suite 1
Las Vegas, NV 89120

1 Eric Anderson
Mountain West Research-Southwest Inc.
2901 N. Central Ave. #1000
Phoenix, AZ 85012-2730

1 Department of Comprehensive Planning
Clark County
225 Bridger Avenue, 7th Floor
Las Vegas, NV 89155

1 Planning Department
Nye County
P.O. Box 153
Tonopah, NV 89049

1 Lincoln County Commission
Lincoln County
P.O. Box 90
Pioche, NV 89043

5 Judy Foremaster
City of Caliente
P.O. Box 158
Caliente, NV 89008

1 Economic Development Department
City of Las Vegas
400 East Stewart Avenue
Las Vegas, NV 89109

1 Community Planning & Development
City of North Las Vegas
P.O. Box 4086
North Las Vegas, NV 89030

1 City Manager
City of Henderson
Henderson, NV 89015

1 Director of Community Planning
City of Boulder City
P.O. Box 367
Boulder City, NV 89005

1 Commission of the European
Communities
200 Rue de la Loi
B-1049 Brussels
Belgium

5 James R. Connolly
Dept. of Geology/Inst. of Meteoritics
University of New Mexico
Albuquerque, NM 87131

1 Troy Soos
Holometrix, Inc.
99 Erie Street
Cambridge, MA 02139

1	6300	T. O. Hunter, Actg.
1	6310	T. E. Blejwas, Actg.
1	6310A	L. E. Shephard
1	6311	A. L. Stevens
1	6312	F. W. Bingham
1	6313	L. S. Costin
1	6313	E. E. Ryder
5	6315	F. B. Nimick, Actg.
1	6316	R. P. Sandoval
1	6317	S. Sinnock
2	6318	L. J. Erickson for 100/1232711/SAND88-3050/QA
1	6318	C. Crawford for Accession No. Data Base
1	6319	R. R. Richards
5	3141	S. A. Landenberger
8	3145	Document Processing for DOE/OSTI
3	3151	G. L. Esch
20	6341	WMT Library
1	6410	D. J. McCloskey, Actg.
1	8523	Technical Library

The number in the lower right-hand corner is an accession number used for Office of Civilian Radioactive Waste Management purposes only. It should not be used when ordering this publication.

Org.	Bldg.	Name	Rec'd by	Org.	Bldg.	Name	Rec'd by

Sandia National Laboratories